Gondwana Research 20 (2011) 745–763

Contents lists available at ScienceDirect

Gondwana Research

journal homepage: www.elsevier.com/locate/gr

The thermo-tectonic history of the Song-Kul plateau, Kyrgyz Tien Shan: Constraints by apatite and titanite thermochronometry and zircon U/Pb dating

Johan De Grave [a,*], Stijn Glorie [a], Mikhail M. Buslov [b], Andrei Izmer [c], Alena Fournier-Carrie [b], Vladislav Yu. Batalev [d], Frank Vanhaecke [c], Marlina Elburg [a], Peter Van den haute [a]

[a] Department of Mineralogy and Petrology, Ghent University, Krijgslaan 281/S8, B-9000 Ghent, Belgium
[b] Institute of Geology and Mineralogy, Siberian Branch, Russian Academy of Sciences, Koptyuga Prospect 3, 630090 Novosibirsk, Russian Federation
[c] Department of Analytical Chemistry, Ghent University, Krijgslaan 281/S12, B-9000 Ghent, Belgium
[d] International Research Center, Russian Academy of Sciences, Bishkek, 720049, Kyrgyzstan

ARTICLE INFO

Article history:
Received 8 November 2010
Received in revised form 29 March 2011
Accepted 31 March 2011
Available online 14 April 2011

Handling Editor: I. Safonova

Keywords:
Tectonics
Zircon U/Pb dating
Thermochronology
Song-Kul
Tien Shan

ABSTRACT

The Song-Kul Basin sits on a plateau at the Northern and Middle Kyrgyz Tien Shan junction. It is a lacustrine basin, occupied by Lake Song-Kul and predominantly developed on igneous basement. This basement was targeted for a multi-method chronological study to identify the different magmatic episodes responsible for basement formation and to constrain the timing of the development of its present-day morphology. Zircon U/Pb dating by LA-ICP-MS revealed four different magmatic episodes: a Late Cambrian (~500 Ma) island arc system, a Late Ordovician (~450 Ma) subduction related intrusion, an Early Permian (~290 Ma) collisional stage, and a Middle to Late Permian (~260 Ma) post-collisional magmatic pulse. Middle to Late Triassic (~200–230 Ma) titanite fission-track ages and Late Triassic – Early Jurassic (~180–210 Ma) apatite fission-track ages and thermal history modeling indicate the Song-Kul basement was already emplaced in the shallow crust at that time. An exhumed fossil apatite fission-track partial annealing zone is recognized in the bordering Song-Kul mountain ranges. The area experienced only minor post-Early Mesozoic denudation. The igneous basement was slowly brought to apatite (U–Th)/He retention temperatures in the Late Cretaceous–Palaeogene. Miocene to present reactivation of the Tien Shan does not manifestly affect this part of the orogen.

1. Introduction and geological setting

Lake Song-Kul is the second largest lake in the Republic of Kyrgyzstan, after Lake Issyk-Kul. It is an endorheic mountain lake of 18 by 29 km, with a shallow maximum depth of 13 m. It is situated at an elevation of 3016 m. The lake occupies an intramontane sedimentary basin of roughly twice the current lake surface, the Song-Kul Basin. It is filled by Late Cenozoic lacustrine sediments. The basin catches these sediments from the bordering mountain ranges that entrap it almost completely. To the north the Song-Kul Basin is limited by the Song-Kul and Kyzart Range (with a ridge crest at about 3200–3500 m), in the south by the Bauralabas and Moldo Range (with a ridge crest at about 3400–3800 m) (Fig. 1). Further to the south the Moldo Range gives way to the Naryn Basin, where elevations drop to around 1700 m at the Naryn River. In the north the Song-Kul and Kyzart Ranges cut off the Song-Kul Basin from the Kochkor Basin (northeast) and the Jumghal Basin (northwest), both at elevations of about 1900 m (Fig. 1). Due to this specific morphology, the Song-Kul Basin essentially represents an internally drained plateau region within the Kyrgyz Tien Shan.

The Tien Shan (or Tianshan, Tian Shan - translated into “Celestial” or “Heavenly” Mountains from Chinese) are part of the Central Asian Orogenic Belt (CAOB). The eastern segment of the Tien Shan is located in China, while most of the western segment (including the Song-Kul area) is situated in the Republic of Kyrgyzstan (Fig. 1). The CAOB is a Palaeozoic accretionary orogen, composed of several Precambrian and Palaeozoic units that amalgamated between Siberia, Baltica and Tarim due to progressive closure of several oceanic basins from the Palaeo-Asian Ocean (Windley et al., 2007; Xiao et al., 2010). The composing units are mainly peri-Gondwanan fragments and island arc systems. In the Permian, the accretionary tectonics of the CAOB reached its peak and all major composing units were joined. Late- and post-orogenic deformation and magmatism further shaped the CAOB basement architecture as a whole and the ancestral Tien Shan in particular (e.g. Xiao et al., 2009). After final construction, the Tien Shan region of the CAOB was subjected to several phases of Mesozoic deformation and was again reactivated in the Late Cenozoic as a distant effect of India–Eurasia collision (e.g. Molnar and Tapponnier, 1975; De Grave et al., 2007). These reactivation episodes in which tectonic inheritance and basement structure play a prominent role, occurred in an intracontinental setting, as distant effects of processes and events transpiring at the margins of the Asian continent (e.g. Allen and Vincent, 1997).

* Corresponding author. Fax: +32 9 2644984.
E-mail address: Johan.DeGrave@UGent.be (J. De Grave).

1342-937X/$ – see front matter
doi:10.1016/j.gr.2011.03.011

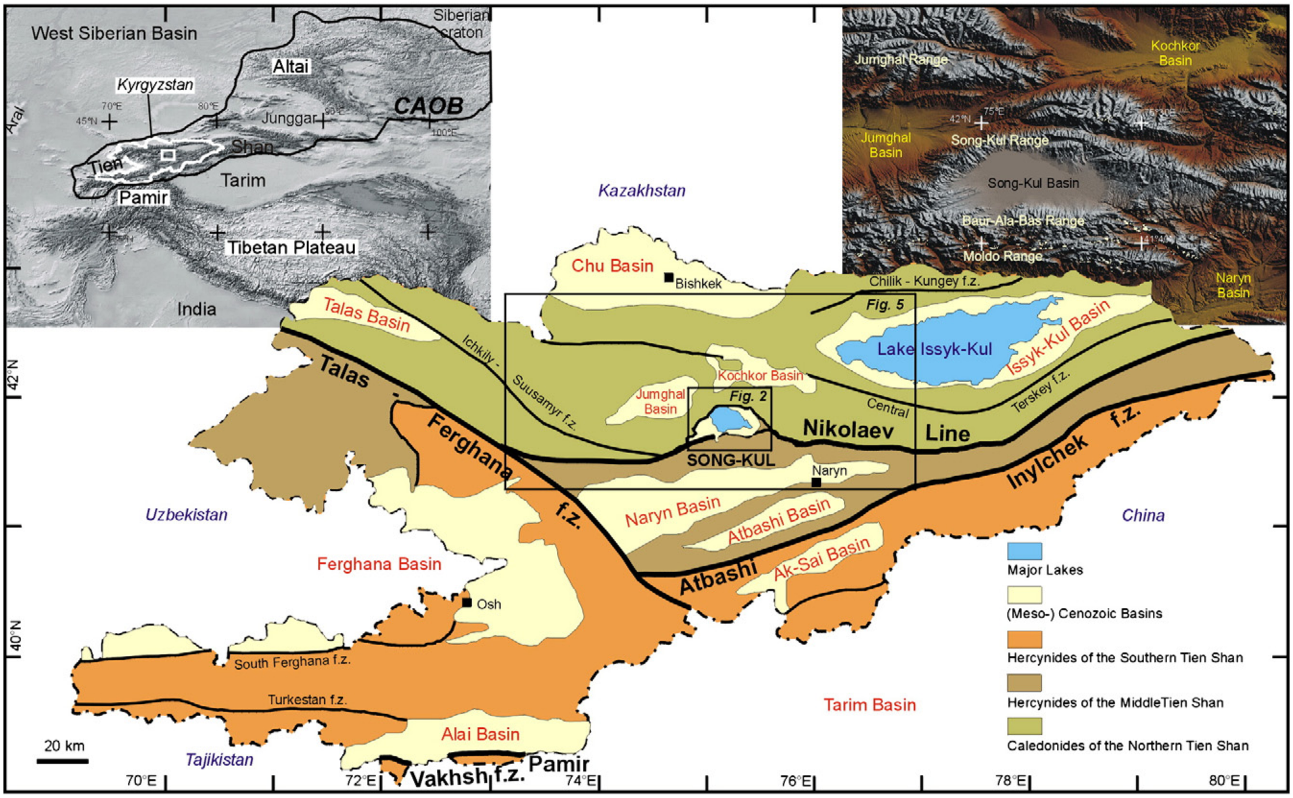

Fig. 1. Palaeozoic terrane subdivision within the Kyrgyz Tien Shan: Northern, Middle and Southern Tien Shan with indication of major basins (Meso-Cenozoic) and basement structures (based on Jenchuraeva et al., 2001). The Song-Kul study area is highlighted: positions for Figs. 2 and 5 are indicated by the boxes. Top left inset: general location of the Tien Shan in the Central Asian Orogenic Belt (CAOB). Top right inset: digital elevation model (SRTM data) of the Song-Kul study area.

The Kyrgyz Tien Shan orogen is traditionally divided in three east–west trending units: the Northern (NTS), Middle (MTS) and Southern Tien Shan (STS) (Fig. 1; e.g. Biske and Seltmann, 2010). The NTS basement is primarily formed by Precambrian micro-continental crust with Cambrian–Ordovician ophiolites on which Palaeozoic continental magmatic arcs and Meso-Cenozoic basins developed. The NTS is vastly intruded by Early Palaeozoic ("Caledonian") granitoids (predominantly Late Ordovician to Early Silurian granites) as well as by smaller, more isolated Late Palaeozoic ("Hercynian") post-collisional plutons (Mikolaichuk et al., 1997; Konopelko et al., 2008; Glorie et al., 2010a). The NTS is separated from the MTS by the Nikolaev Line (e.g. Biske and Seltmann, 2010, and references therein). The MTS basement is mainly composed of Precambrian crust with Neoproterozoic volcanic rocks and tillites, and is considered to be associated with Peri-Gondwanan micro-continents (Biske and Seltmann, 2010). This basement is covered by Early Palaeozoic sediments and by Middle Palaeozoic (Middle Devonian–Early Carboniferous) passive margin sequences linked to the Early Palaeozoic composite palaeo-Kazakhstan passive margin. In contrast to the NTS, Early Palaeozoic granitoids appear to be absent in the MTS, while Late Palaeozoic post-collisional plutons are prevalent (e.g. Mao et al., 2004; Seltmann et al., in press). To the south the MTS is separated from the STS by the ophiolite-bearing Atbashi-Inylchek suture (or South Tien Shan Suture, e.g. Jenchuraeva et al., 2001). The STS represents a Late Palaeozoic collision-accretion system characterized by a complex fold-and-thrust structure mainly involving Silurian to Lower Permian sedimentary and volcanic rocks (Alekseev et al., 2007; Biske and Seltmann, 2010).

The Song-Kul Basin is situated at the junction zone between the NTS and MTS in Central Kyrgyzstan (Fig. 1). The basin developed mainly on granitoids and volcanic rocks of both "Caledonian" and "Hercynian" affinity. This basement that supports the Song-Kul Basin, is referred to in this paper as the Song-Kul block. The previous observations would argue for the fact that at least part of the "Song-Kul block" is a section of the NTS and that this is hence situated north of the Nikolaev Line, while the majority of the block is an element of the MTS. This is not always clear in literature; most authors indeed position Song-Kul north of the Nikolaev Line, in the NTS (e.g. Jenchuraeva et al., 2001; Maksumova et al., 2001; Omuralieva et al., 2009), while in some studies it is completely included in the MTS, south of the Nikolaev Line (e.g. Windley et al., 2007; Konopelko et al., 2008; Gao et al., 2009; Alekseev et al., 2009). The Nikolaev Line is then drawn in between the Ordovician granitoids north and west of the Song-Kul Basin, around the basin and the Carboniferous–Permian granitoids (mostly to the east and south of the basin; Fig. 2). Sometimes it is traced cutting through the Song-Kul Basin itself with Ordovician granitoids to the north and the Carboniferous–Permian rocks to the south (e.g. Tursungaziev and Petrov, 2008). In yet other cases the Song-Kul Basin is drawn in between the Nikolaev line to its south and a branched fault to its north (e.g. Mikolaichuk et al., 1997; Burbank et al., 1999; Solomovich, 2007). It lies outside the scope of this paper to resolve this question, but it is clear from the modern morphology (Fig. 3) and the geology (Fig. 2) that the Song-Kul Plateau currently behaves as a single block with a clear boundary fault to its south, along the Moldo Range. Further to the west, towards the Talas-Ferghana fault, the Nikolaev Line is traced along the Moldo Range.

2. Samples and methodology

Sample details including locations and lithology and the methods applied in this study are listed in Table 1. Their positions are plotted on a simplified geological map and terrain model (Figs. 2 and 3). All but one sample from the Song-Kul area are from Palaeozoic granites and diorites. The one other sample (AI-92) originates from a biotite-bearing lamprophyre dyke in a larger granitic pluton north of the Song-Kul Basin, near Kyzart pass. Granite sample AI-91 represents the

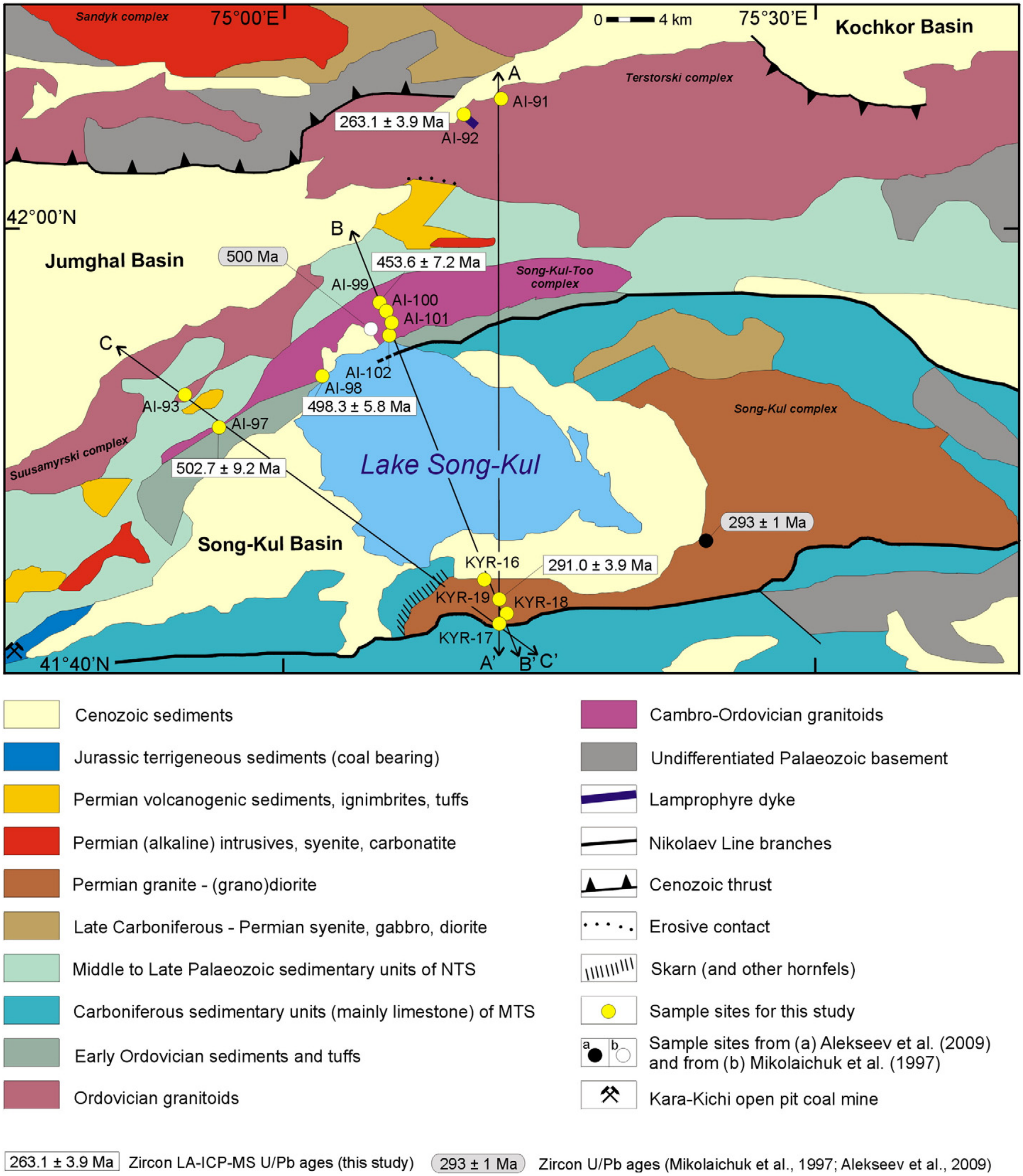

Fig. 2. Simplified geological map of the Song-Kul area in the Northern Kyrgyz Tien Shan (based on Tursungaziev and Petrov, 2008) with indication of sample sites and zircon U/Pb dating results. See Fig. 1 for general location. Locations of the topographic profiles (A–A′, B–B′ and C–C′) depicted in Fig. 6 are shown.

host rock for the AI-92 dyke. Based on maps by Jenchuraeva et al. (2001) and Tursungaziev and Petrov (2008) this is an igneous complex, the Terstorski complex, consisting of Middle Ordovician I-type diorites and granodiorites, and Late Ordovician S-type granodiorites and granites as indicated on the map. AI-91 is a granite sample from the latter. These Late Ordovician S-type granitoids also crop out west of Lake Song-Kul (Fig. 2), where they represent the easternmost termination of the large Suusamyrski complex that stretches to the Talas-Ferghana fault to the west (Fig. 1). Carboniferous and Permian rocks are found on top of the Suusamyrski granites, along an erosional contact (Fig. 2). Granite

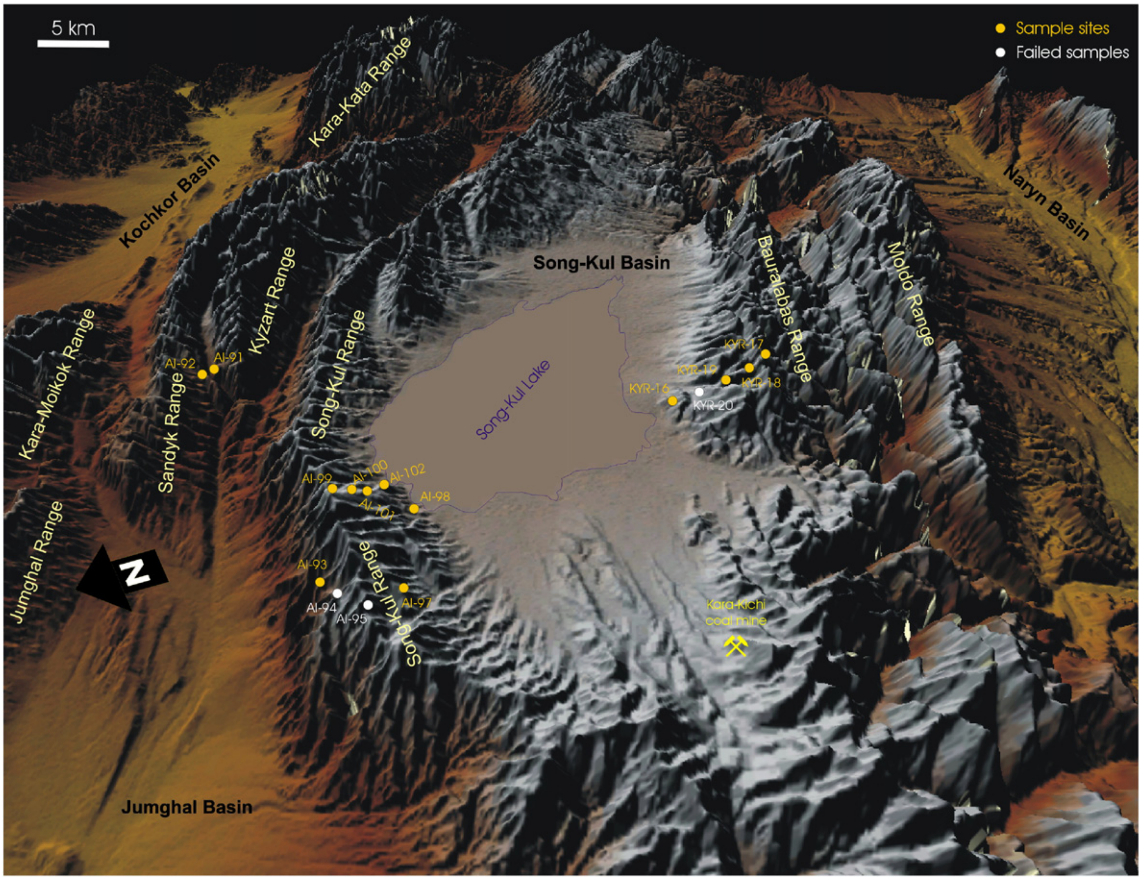

Fig. 3. Digital elevation model of the "Song-Kul block", looking in eastward direction (WGS84 frame, SRTM data). Morphological features and sample sites are indicated. See inset of Fig. 1 for location and position.

sample AI-93 comes from this eastern section of the Suusamyrski complex. The Jumghal Basin separates these Ordovician granitoids (incl. AI-93) from their counterparts north of the Song-Kul Basin, where samples AI-91 and AI-92 were collected. The basin-vergent side of the bordering Song-Kul Range is primarily built by the Late Cambrian–Early Ordovician Song-Kul-Too (quartz-)diorites, tonalites and gabbros. These intrusions are considered to be the root of a Late Cambrian–Early Ordovician island arc that was attached during subduction of the so-called Ishim-Naryn branch of the Paleo-Asian Ocean (Jenchuraeva, 2001). In this complex, west to northwest of the Song-Kul Basin, diorite samples AI-97 to AI-102 were collected along a vertical transect of about 500 m altitude difference (Fig. 2). These diorites are very close to tonalite in composition. South and east, the Song-Kul Basin covers the Early Permian multistage Song-Kul igneous complex. The outcrops of this complex are situated in the central and eastern segments of the Bauralabas Range. The first intrusion stage of this complex is represented mainly by gabbroids, diorites and monzonites (phase 1, Jenchuraeva, 2001; Alekseev et al., 2009). Quartz monzonites, and quartz (monzo)diorites represent a second phase, while the third and most voluminous phase includes granites, granodiorites and granosyenites. Our sample transect in the Bauralabas mountain range (samples KYR-16 to KYR-19) includes granites from this terminal intrusion stage of the Song-Kul igneous complex.

To a large extent, the Song-Kul Basin developed on this igneous basement, compiled from these Early to Late Palaeozoic complexes. To understand the specific plateau-like morphology and relief of the

Table 1
Sample location and lithology details and indication of applied methods (AFT = Apatite Fission-Track dating, AHe = Apatite (U–Th–Sm)/He dating, TFT = Titanite Fission-Track dating, ZUPb = Zircon U/Pb dating).

Sample	Latitude	Longitude	Alt.	Range/Region	Lithology	Method
AI-91	N42°05′35″	E075°07′11″	2572 m	Sandyk Range	Granite	AFT, AHe
AI-92	N42°05′03″	E075°04′41″	2438 m	Sandyk Range	Lamprophyre	AFT, ZUPb
AI-93	N41°53′51″	E074°49′25″	2290 m	Song-Kul Range	Granite	AFT
AI-97	N41°50′37″	E074°54′04″	3253 m	Song-Kul Range	Diorite	AFT, AHe, ZUPb
AI-98	N41°53′06″	E075°01′05″	3046 m	Song-Kul Range	Diorite	AFT, ZUPb
AI-99	N41°55′56″	E075°01′44″	3514 m	Song-Kul Range	Diorite	AFT, TFT
AI-100	N41°55′41″	E075°02′15″	3364 m	Song-Kul Range	Diorite	AFT, AHe, ZUPb
AI-101	N41°55′08″	E075°02′21″	3212 m	Song-Kul Range	Diorite	AFT
AI-102	N41°54′36″	E075°02′48″	3066 m	Song-Kul Range	Diorite	AFT, AHe
KYR-16	N41°45′41″	E075°09′38″	3090 m	Bauralabas Range	Granite	AFT, TFT
KYR-17	N41°43′01″	E075°11′19″	3720 m	Bauralabas Range	Granite	AFT
KYR-18	N41°43′44″	E075°11′26″	3535 m	Bauralabas Range	Granite	TFT
KYR-19	N41°44′16″	E075°11′22″	3400 m	Bauralabas Range	Granite	TFT, ZUPb

Table 2
Analytical details for the LA-ICP-MS zircon U/Pb dating used in this study. Two settings were applied (a) for samples AI-97 and KYR-19; (b) for samples AI-92, AI-98 and AI-100.

ICP-MS	
Brand and model	ThermoFinnigan Element XR (Sector-field MS)
Forward power	800–1000 W
Gas flows (l/min)	
Cool (Ar)	~16.0
Auxiliary (Ar)	~1.0
Carrier (He)	0.3–0.35
Sample (Ar)	0.8–0.85
Laser	
Type of Laser	ArF-Excimer
Brand and model	[a]New Wave UP 193 [b]MicroLas GeoLas M LA
Ablation cell	[a]Teardrop-shaped low-volume cell (<2.5 cm³) [b]Standard cell (~30 cm³)
Laser wavelength	193 nm
Spot size	30 μm
Repetition rate	10 Hz
Pulse duration	5 ns
Nominal energy output	40–45%
Laser fluency	[a]2.5–3.0 J cm^{-2}, [b]4.0–4.5 J cm^{-2}
Laser warm up (background collection)	[a]25 s, [b]40 s
Ablation time	[a]40 s (400 pulses), [b]30 s (300 pulses)
Wash-out	[a]25 s, [b]120 s
Data acquisition parameters	
Resolution mode	Low
Data acquisition protocol	Time-resolved analysis
Scan mode	E-scan
Scanned masses	202 (Hg), 204 (Hg, Pb), 206 (Pb), 207 (Pb), 208 (Pb), 232 (Th), 235 (U), 238 (U)
Detector deadtime	18 ns
Background collection	[a]25 s, [b]40 s
Ablation for age calculation	[a]40 s, [b]30 s
Wash-out collection	[a]15 s, [b]120 s
Standardization and data reduction	
Reference standard used	GJ-1
Secondary standard used	Plešovice
Data reduction software used	PepiAGE (Dunkl et al., 2009) + In house Excel-spreadsheet

Song-Kul Basin in an absolute thermo-tectonic time frame, and to constrain the exact timing of the different intrusions phases, the samples were subjected to several geochronological and thermochronological techniques. Zircon U/Pb dating (ZUPb) using LA-ICP-MS (Laser Ablation-Inductively Coupled Plasma-Mass Spectrometry) was performed to obtain the crystallization ages of the individual plutons and to obtain a high-temperature bench mark for subsequent thermochronology analysis of the basement. Absolute radiometric age information from this region is scarce and for a large part based on the K–Ar method. Where available this age information is often ambiguous (as e.g. mentioned in Alekseev et al., 2009). This study presents new ZUPb ages for the granitoid bodies, described above. Titanite (TFT) and Apatite (AFT) Fission-Track thermochronology are used to characterize the thermal history of the basement in the upper reaches of the crust. For some samples the Apatite (U–Th–Sm)/He (AHe) thermochronometer was used to further constrain the cooling and hence denudation of the basement during the Meso-Cenozoic reactivation events that characterize the Tien Shan. Analytical procedures for all these techniques are briefly outlined below.

2.1. Zircon U/Pb dating by LA-ICP-MS

Zircons were dated with the U/Pb method using Laser Ablation-Inductively Coupled Plasma-Mass Spectrometry (LA-ICP-MS) at the Department of Analytical Chemistry, Ghent University and procedures are nearly identical to those described in Glorie et al. (2011) and De Grave et al. (in press). Table 2 gives an overview of analytical details. Two laser systems were used: a New Wave UP193HE and a MicroLas GeoLas M LA excimer-based laser ablation system (Table 2) with a teardrop-shaped low-volume (<2.5 cm³) ablation cell that was coupled to the ICP-mass spectrometer. U(−Th)/Pb isotopic ratios were determined using a Thermo Scientific Element XR Sector Field ICP-MS instrument. Laser-induced elemental fractionation was corrected for by using the arithmetic mean ratio for each run. Instrumental mass discrimination was corrected for by normalization to the reference zircon GJ-1 (Jackson et al., 2004). Drift-correction was calculated by applying a linear fit through the measured ratios for the GJ-1 standard. Concordia ages were calculated with the Isoplot software (Ludwig, 2003). Plešovice (Sláma et al., 2008) and 91500 (Wiedenbeck et al., 1995) secondary zircon standards were analyzed multiple times throughout each measurement sequence as an accuracy check. A long-term (n = 98, spread over several measurement days) concordia age for the Plešovice secondary standard in our measurements was calculated at 338.3 ± 1.5 Ma, compared to the published ID-TIMS age of 337.1 ± 0.4 Ma (Sláma et al., 2008).

2.2. Titanite fission-track dating

Sample mounts for TFT dating were prepared and provided with a muscovite (Goodfellow, clear ruby) external detector (ED) in the same way as done for the AFT mounts described below. Spontaneous tracks were etched with a 0.4% HF solution for 24 h at 20 °C (Jonckheere and Wagner, 2000a; 2000b; Enkelmann et al., 2005), induced tracks in the muscovite ED with 40% HF for 40 min at 20 °C (temperature controlled in a thermostatic bath). Irradiation was performed at the Belgian Reactor 1 (BR1) facility of the Belgian Nuclear Research Centre in Mol in channel X26 (De Grave et al., in press). A thermal neutron fluence of 2.17×10^{15} cm^{-2} was achieved and monitored using metal activation monitors (Co–Al and Au–Al foils). As for the AFT method (below), counting was performed using an Olympus BH-2 microscope (1250× magnification) equipped with transmitted and reflected light and drawing tube attachment. The repositioning technique by Jonckheere et al. (2003) was used. While absolute calibration of the thermal neutron fluence allows for using the absolute age equations (Wagner and Van den haute, 1992; Enkelmann et al., 2005), a zeta (ζ) calibration approach using the titanite age standards of Mount Dromedary and Fish Canyon Tuff (Williams et al., 1982; Green, 1985) was also applied here. ζ-values were determined against the IRMM-540 dosimeter glass (De Corte et al., 1998). Calibration, counting and ζ-calculation details are shown in Table 3. An overall weighted mean zeta (OWMZ) of 505.1 ± 7.8 a cm² was obtained (based on Fish Canyon Tuff and Mount Dromedary titanite age standards) and used for the age determination of the Song-Kul titanite samples. Standards and samples were irradiated in a single batch. All titanite mounts and all ED micas were etched in a single bath, under identical conditions. Induced glass dosimeter track densities (ρ_d) were calculated through interpolation as done for the AFT method (below). Absolute calibration of the TFT ages was performed using the absolute thermal neutron fluence value of 2.17×10^{15} cm^{-2} as outlined above, and the recommended value of 8.46×10^{-17} a^{-1} for the ^{238}U fission decay constant (Galliker et al., 1970; Wagner and Van den haute, 1992; Enkelmann et al., 2005). Based on these values and on Fish Canyon Tuff and Mount Dromedary titanite standards, a procedure factor (Q-factor, Wagner and Van den haute, 1992) of 1.910 ± 0.070 was calculated.

2.3. Apatite fission-track thermochronometry

The traditional ED method with thermal neutron irradiation was used. Details on the procedures in our laboratory can be found in De

Table 3
Zeta (ζ) values (in a.cm²) for TFT analyses based on both Fish Canyon Tuff titanite (sphene) standards (FCS) and Mount Dromedary titanite (sphene) standards (MDS) with a standard age of 27.8 ± 0.2 Ma (Williams et al., 1982) and 98.8 ± 0.6 Ma (Green, 1985) respectively. The number of analyzed grains is given by n. The spontaneous, induced and glass dosimeter track densities (ρ_s, ρ_i, ρ_d respectively) are all expressed as 10^6 tracks/cm² and based on counting N_s, N_i and N_d tracks. The IRMM-540 dosimeter glass (De Corte et al., 1998) was used for calculation of the associated zeta values (ζ_{540}). P(χ^2) probabilities are expressed in %. S(O)WMZ = Standard (Overall) Weighted Mean Zeta.

Sample	n	ρ_s	N_s	ρ_i	N_i	P(χ^2)	ρ_d	N_d	ζ_{540}	SWMZ	OWMZ
FCS-2	25	0.387	1237	1.463	4682	55.82	0.405	2591	515.5 ± 19.7		
FCS-3	20	0.414	1060	1.564	4003	95.41	0.398	2544	523.0 ± 21.2	519.0 ± 14.4	
MDS-1	15	3.708	2283	3.820	2326	79.13	0.403	2581	506.4 ± 18.2		
MDS-2	15	4.102	2083	4.169	2147	5.87	0.405	2591	505.0 ± 18.7		
MDS-3	15	3.698	2158	3.572	2128	10.72	0.398	2544	490.2 ± 18.1		
MDS-4	14	4.809	2077	4.827	2099	73.71	0.397	2541	496.1 ± 18.5	499.4 ± 9.2	505.1 ± 7.8

Grave et al. (2008, 2009) for example, and are briefly outlined below. Spontaneous tracks were etched with a 2.5% HNO_3 solution for 70 s at 25 °C, induced tracks in the ED with 40% HF for 40 min at 20 °C. Irradiation was also done at BR1 in channel X26. Most samples were irradiated in a single package with a thermal neutron fluence of 2.16×10^{15} cm^{-2}; monitored using metal activation monitors. Samples AI-98 and KYR-16 were irradiated in a second batch with a thermal neutron fluence of 2.23×10^{15} cm^{-2}. Sample KYR-17 was irradiated earlier in the now decommissioned Thetis reactor of Ghent University (De Grave et al., 2008; Glorie et al., 2010a) with a thermal neutron fluence of 1.70×10^{15} cm^{-2}. AFT ages are reported as conventional ζ-ages (Hurford, 1990) although absolute ages are generally identical within analytical uncertainty (e.g. De Grave and Van den haute, 2002; Glorie et al., 2010a). An overall weighted mean zeta of 253.1 ± 2.4 a cm² (Durango and Fish Canyon Tuff apatite standards) for the IRMM-540 dosimeter glass (De Corte et al., 1998) is used. Dosimeter glass was regularly spaced in the sample package to detect and correct for any axial thermal neutron fluence gradient and to allow interpolation of induced glass dosimeter track densities (ρ_d) for individual samples. Where possible 100 natural horizontal confined tracks were measured to construct an AFT length–frequency distribution (Gleadow et al., 1986).

2.4. Apatite (U–Th–Sm)/He thermochronometry

The Apatite (U–Th–Sm)/He (AHe) method is an ideally suited complementary technique to AFT. While sample preparation was carried out in our facilities, AHe analysis was performed at the (U–Th)/He laboratory of Kansas State University (USA) and analytical procedures are described in detail e.g. by Blackburn et al. (2008) and De Grave et al. (in press). Carefully selected grains were loaded in separate platinum sleeves and three duplicate aliquots were prepared. α-ejection correction was done based on the F_T ejection correction method (Farley, 2002; Farley et al., 1996). Sample aliquots were heated by a 20 W Nd-YAG laser to fuse the grains and evacuate the ^{4}He gas. The resulting ^{4}He was measured by isotope dilution (^{3}He spike), after gettering and cryogenic purification, with a Blazers Prisma QMS-200 quadrupole mass spectrometer. After dissolution, U, Th and Sm concentrations were determined by a VG Plasmaquad-2 ICP-MS.

2.5. Thermal history modelling

Thermal history modelling was performed using the HeFTy software (Ketcham, 2005) and the Ketcham et al. (2007) annealing-equations. Where available (Table 1) both AFT and AHe input was provided (except for sample AI-91 that exhibits conflicting AHe and AFT ages), while in other cases only AFT data was used (except for sample AI-92 that did not yield enough confined track lengths). AFT length data goodness of fit was tested with the Kolmogorov–Smirnov test (Ketcham, 2005). The Monte Carlo search method was adopted for inverse modelling. For each sample 50,000 paths were calculated and yielded at least several hundred to in some cases more than 2000 "good" time-Temperature (tT) paths (Ketcham, 2005). Constraints (tT boxes) were only placed based on geological arguments such as ZUPb intrusion ages, and TFT, AFT and AHe ages from this study. No c-axis projection was employed for modelling because our etching conditions show a more isotropic trend in comparison to the c-axis projection equations embedded in the HeFTy program (Glorie et al., 2010b). We used a fixed l_o-value of 16.05 μm, following our laboratory specific induced confined track length calibration (age standards and "geological samples").

3. Results and discussion

3.1. Zircon U/Pb dating by LA-ICP-MS

Results from the zircon U/Pb dating by LA-ICP-MS are presented in Table 4 and corresponding concordia plots and age results are presented in Fig. 4. Ages are also indicated on the map in Fig. 2. Fig. 5 provides an overview of ZUPb ages obtained from the NTS/MTS granitoids in order to situate our results in a broader context. Here and elsewhere we follow the 2009 geological timescale by the International Commission on Stratigraphy, based on the Gradstein et al. (2004) timescale. For local correlations the Tursungaziev and Petrov (2008) 1:500,000 scale geological map and 1:200,000 scale geological maps of the Kyrgyz Ministry of Geology were used (map sheets K-43-15, K-43-16, K-43-21, and K-43-22).

Two distinct age groups can be distinguished in our data: an Early and a Late Palaeozoic age group. Samples AI-97 (502.7 ± 9.2 Ma), AI-98 (498.3 ± 5.8 Ma), and AI-100 (453.6 ± 7.2 Ma) represent the Early Palaeozoic group. These samples are all from the Song-Kul-Too (quartz) diorites (near tonalite in composition). According to recently published geological maps, the Song-Kul-Too complex is of Middle Cambrian to Early Ordovician age (Jenchuraeva et al., 2001), while Tursungaziev and Petrov (2008) constrain it to the Early Ordovician. On older 1:200,000 geological maps published by the former Soviet Ministry of Geology in the 1960s (Map Sheet K43-22), this intrusive complex is mapped as Late Ordovician with a "?". Our results show that the diorites from the Song-Kul-Too complex have ZUPb crystallization ages between ~503 and 454 Ma (Late Cambrian to earliest Late Ordovician). However a marked difference is noticeable between samples from the southwestern area (AI-97 and AI-98) and sample AI-100 from the central transect (Fig. 2). While the latter gives an earliest Late Ordovician age of ~454 Ma (Sandbian), the former samples are significantly older at about 503–498 Ma (Late Cambrian, Guzhangian–Paibian transition). At this moment we have no clear explanation for this discrepancy and additional geochemical data is required and underway (Konopelko, pers. comm.). Investigation by optical petrographic microscopy on thin sections does not indicate different lithologies or mineral associations. All sampled rocks are fresh and do not show signs of alteration. Nor is there any clear field evidence to conclude that the samples come from different igneous bodies or different phases of intrusion. The only marked difference observed at the AI-100 outcrop was the presence of large amounts of pyroxenite xenoliths. Also the size, colour, morphology and the oscillatory magmatic zonation of the zircons from samples AI-97 and AI-98 on one hand and AI-100 on the other, does not show significant

Table 4
Zircon U/Pb dating results by LA-ICP-MS. In bold below: arithmetic mean values of all tabulated parameters for each sample.

	n°	$^{207}Pb^{a}$ (cps)	U^{b} (ppm)	Pb^{b} (ppm)	$\frac{Th_b}{U}$	$\frac{^{206}Pb}{^{204}Pb}$	$\frac{^{206}Pb_c}{^{238}U}$	±2σ (%)	$\frac{^{207}Pb_c}{^{235}U}$	±2σ (%)	$\frac{^{207}Pb_c}{^{206}Pb}$	±2σ (%)	rho[d]	$\frac{^{206}Pb_e}{^{238}U}$	±2σ (Ma)	$\frac{^{207}Pb_e}{^{235}U}$	±2σ (Ma)	con.[f]
AI-97	1	3491	267	22	0.25	740	0.0809	5.0	0.6583	7.3	0.0590	5.3	0.69	501	24	514	30	102
	2	3332	255	21	0.27	2165	0.0811	5.4	0.6703	8.3	0.0600	6.3	0.65	503	26	521	34	104
	3	3370	264	21	0.27	2658	0.0786	3.4	0.6723	7.1	0.0620	6.2	0.49	488	16	522	29	107
	4	2162	169	14	0.20	1083	0.0828	5.0	0.7094	10.0	0.0621	8.6	0.50	513	25	544	43	106
	5	2709	210	18	0.27	604	0.0820	4.2	0.6890	7.8	0.0610	6.6	0.54	508	20	532	33	105
	6	3150	276	21	0.21	986	0.0775	4.6	0.6080	6.8	0.0569	5.0	0.68	481	21	482	26	100
	7	4743	361	31	0.35	663	0.0829	5.4	0.7331	11.0	0.0642	9.6	0.49	513	26	558	48	109
	8	2660	210	18	0.35	2058	0.0836	4.1	0.7026	7.6	0.0609	6.4	0.54	518	20	540	33	104
	9	3785	311	26	0.29	679	0.0814	6.0	0.6553	9.6	0.0584	7.5	0.63	504	29	512	39	101
	10	1984	162	13	0.25	286	0.0812	3.9	0.6787	7.7	0.0606	6.7	0.50	504	19	526	32	104
	11	1846	156	13	0.21	597	0.0804	3.8	0.6781	10.5	0.0611	9.8	0.36	499	18	526	44	105
AI-98	1	1953	158	13	0.23	530	0.0841	4.4	0.6443	7.0	0.0556	5.4	0.63	520	22	505	28	97
	2	967	84	7	0.33	3029	0.0815	3.7	0.5999	9.0	0.0534	8.2	0.41	505	18	477	35	94
	3	1360	114	9	0.18	488	0.0791	3.0	0.6185	8.0	0.0567	7.4	0.37	491	14	489	31	100
	4	2179	188	17	0.46	12524	0.0805	3.5	0.6765	8.3	0.0610	7.5	0.42	499	17	525	35	105
	5	1346	112	9	0.26	334	0.0804	3.5	0.6448	7.0	0.0582	6.1	0.50	498	17	505	28	101
	6	1319	112	9	0.24	2323	0.0809	3.6	0.6356	6.9	0.0570	5.9	0.52	501	17	500	28	100
	7	1335	114	10	0.32	606	0.0801	3.7	0.6306	7.6	0.0571	6.6	0.49	497	18	496	30	100
	8	669	56	5	0.25	287	0.0795	3.8	0.6572	9.7	0.0599	8.9	0.39	493	18	513	40	104
	9	610	60	5	0.22	458	0.0798	4.0	0.5746	9.9	0.0522	9.1	0.40	495	19	461	37	93
	10	1353	103	9	0.33	477	0.0827	3.2	0.7351	8.2	0.0644	7.5	0.39	512	16	560	36	109
	11	1136	97	8	0.32	1100	0.0787	3.2	0.6628	7.0	0.0611	6.2	0.46	489	15	516	29	106
	12	1377	123	10	0.20	664	0.0773	3.1	0.6341	6.3	0.0595	5.5	0.49	480	14	499	25	104
	13	821	73	6	0.25	276	0.0807	3.5	0.6599	8.7	0.0593	7.9	0.40	500	17	515	36	103
	14	1210	104	9	0.30	376	0.0814	3.4	0.6568	9.0	0.0586	8.3	0.37	504	16	513	37	102
	15	944	76	7	0.28	595	0.0821	3.5	0.7160	8.1	0.0633	7.3	0.43	509	17	548	35	108
	16	951	88	8	0.37	3304	0.0796	3.9	0.6395	8.2	0.0583	7.2	0.48	494	19	502	33	102
AI-100	1	4431	456	35	0.36	1212	0.0733	2.6	0.5681	4.4	0.0562	3.5	0.59	456	11	457	16	100
	2	3071	319	26	0.41	948	0.0763	3.9	0.5754	6.5	0.0547	5.2	0.60	474	18	462	24	97
	3	3117	346	27	0.46	2391	0.0702	3.3	0.5268	5.0	0.0544	3.8	0.65	437	14	430	18	98
	4	4023	446	33	0.32	938	0.0705	3.3	0.5340	4.9	0.0549	3.6	0.68	439	14	434	17	99
	5	2917	306	25	0.46	971	0.0738	3.2	0.5901	4.9	0.0580	3.8	0.64	459	14	471	19	103
	6	4641	489	37	0.28	6666	0.0739	4.5	0.5904	7.1	0.0580	5.6	0.62	459	20	471	27	103
	7	3957	424	32	0.32	3788	0.0706	4.2	0.5701	7.2	0.0586	5.8	0.59	439	18	458	27	104
	8	3278	342	27	0.33	3160	0.0746	3.0	0.5987	4.9	0.0582	3.9	0.62	464	14	476	19	103
	9	4442	483	37	0.35	1484	0.0733	3.2	0.5715	4.8	0.0566	3.5	0.68	456	14	459	18	101
	10	8800	1099	88	0.48	5658	0.0714	16.3	0.5706	16.8	0.0579	4.3	0.97	445	70	458	64	103
Kyr-19	1	3470	357	18	0.45	1309	0.0452	3.7	0.3331	7.5	0.0534	6.5	0.50	285	10	292	19	102
	2	3309	362	19	0.52	506	0.0460	4.3	0.3470	9.1	0.0547	8.0	0.48	290	12	302	24	104
	3	2368	208	11	0.58	1074	0.0457	2.7	0.3605	9.4	0.0572	9.0	0.29	288	8	313	26	108
	4	6235	703	36	0.53	1667	0.0465	4.0	0.3286	5.9	0.0513	4.3	0.68	293	11	288	15	98
	5	5118	616	31	0.54	1777	0.0457	4.5	0.3331	5.9	0.0529	3.8	0.76	288	13	292	15	101
	6	6549	780	40	0.58	1979	0.0458	3.4	0.3262	5.7	0.0516	4.5	0.61	289	10	287	14	99
	7	3231	344	17	0.47	820	0.0461	3.8	0.3569	8.2	0.0562	7.3	0.46	290	11	310	22	107
	8	5910	626	33	0.59	1550	0.0464	3.7	0.3413	6.0	0.0534	4.7	0.61	292	10	298	16	102
	9	6190	627	33	0.55	1337	0.0467	4.7	0.3597	7.3	0.0558	5.6	0.65	294	14	312	20	106
	10	6285	752	38	0.64	2602	0.0454	3.7	0.3323	5.9	0.0531	4.6	0.63	286	10	291	15	102
	11	5178	591	30	0.53	1182	0.0454	4.0	0.3411	5.3	0.0545	3.5	0.75	286	11	298	14	104
	12	3460	411	22	0.63	1858	0.0465	3.9	0.3564	7.0	0.0556	5.8	0.57	293	11	309	19	106
	13	5715	678	35	0.56	9409	0.0471	3.1	0.3537	4.8	0.0545	3.7	0.64	296	9	308	13	104
	14	3793	456	24	0.56	864	0.0480	4.4	0.3658	6.4	0.0553	4.6	0.69	302	13	317	17	105
AI-92	1	1611	346	15	0.36	1080	0.0421	2.7	0.2987	5.9	0.0515	5.3	0.46	266	7	265	14	100
	2	2013	385	17	0.20	979	0.0436	4.1	0.3272	7.8	0.0544	6.6	0.53	275	11	287	20	104
	3	926	205	9	0.23	567	0.0408	3.1	0.2947	7.5	0.0523	6.8	0.41	258	8	262	18	102
	4	779	177	7	0.25	727	0.0409	2.7	0.2900	9.9	0.0514	9.5	0.28	259	7	259	23	100
	5	945	200	9	0.32	340	0.0423	2.8	0.3141	8.1	0.0538	7.6	0.34	267	7	277	20	104
	6	672	160	7	0.25	6844	0.0412	2.7	0.2822	8.5	0.0496	8.1	0.31	261	7	252	19	97
	7	1675	366	16	0.25	744	0.0413	3.0	0.3077	5.8	0.0540	5.0	0.51	261	8	272	14	104
	8	4383	898	39	0.28	1355	0.0415	4.8	0.3329	7.4	0.0582	5.5	0.66	262	12	292	19	111
	9	1042	245	11	0.34	413	0.0416	3.3	0.2951	8.0	0.0515	7.3	0.41	263	9	263	19	100
	10	848	208	9	0.29	373	0.0422	3.1	0.2773	7.7	0.0477	7.1	0.39	267	8	249	17	93
AI-97		**3021**	**240**	**20**	**0.27**	**1138**	**0.0811**	**4.6**	**0.6777**	**8.5**	**0.0606**	**7.1**	**0.55**	**503**	**22**	**525**	**36**	**104**
AI-98		**1221**	**104**	**9**	**0.28**	**1711**	**0.0805**	**3.6**	**0.6491**	**8.1**	**0.0585**	**7.2**	**0.45**	**499**	**17**	**508**	**33**	**102**
AI-100		**4268**	**471**	**37**	**0.38**	**2722**	**0.0728**	**4.7**	**0.5696**	**6.6**	**0.0568**	**4.3**	**0.66**	**453**	**21**	**458**	**25**	**101**
Kyr-19		**4772**	**537**	**28**	**0.55**	**1995**	**0.0462**	**3.9**	**0.3454**	**6.7**	**0.0543**	**5.4**	**0.59**	**291**	**11**	**301**	**18**	**104**
AI-92		**1489**	**319**	**14**	**0.28**	**1342**	**0.0418**	**3.2**	**0.3020**	**7.7**	**0.0524**	**6.9**	**0.43**	**264**	**8**	**268**	**18**	**102**

[a] Within-run, background-corrected mean ^{207}Pb signal.
[b] U and Pb content and Th/U ratio were calculated relative to the GJ-1 zircon standard.
[c] Corrected: background, within-run Pb/U fractionation ($^{206}Pb/^{238}U$) and where needed common Pb (Stacey and Kramers (1975) model Pb composition) and subsequently normalised to GJ-1 (Instrumental drift corrected using a linear fit calibration line). $^{207}Pb/^{235}U$ calculated using $^{207}Pb/^{206}Pb * ^{206}Pb/^{238}U * 137.88$.
[d] rho is the error correlation defined as $err^{206}Pb/^{238}U$ / $err^{207}Pb/^{235}U$.
[e] U/Pb ages were calculated with Isoplot (Ludwig, 2003).
[f] Degree of concordance = $age^{206}Pb/^{238}U$ / $age^{207}Pb/^{206}Pb \times 100$.

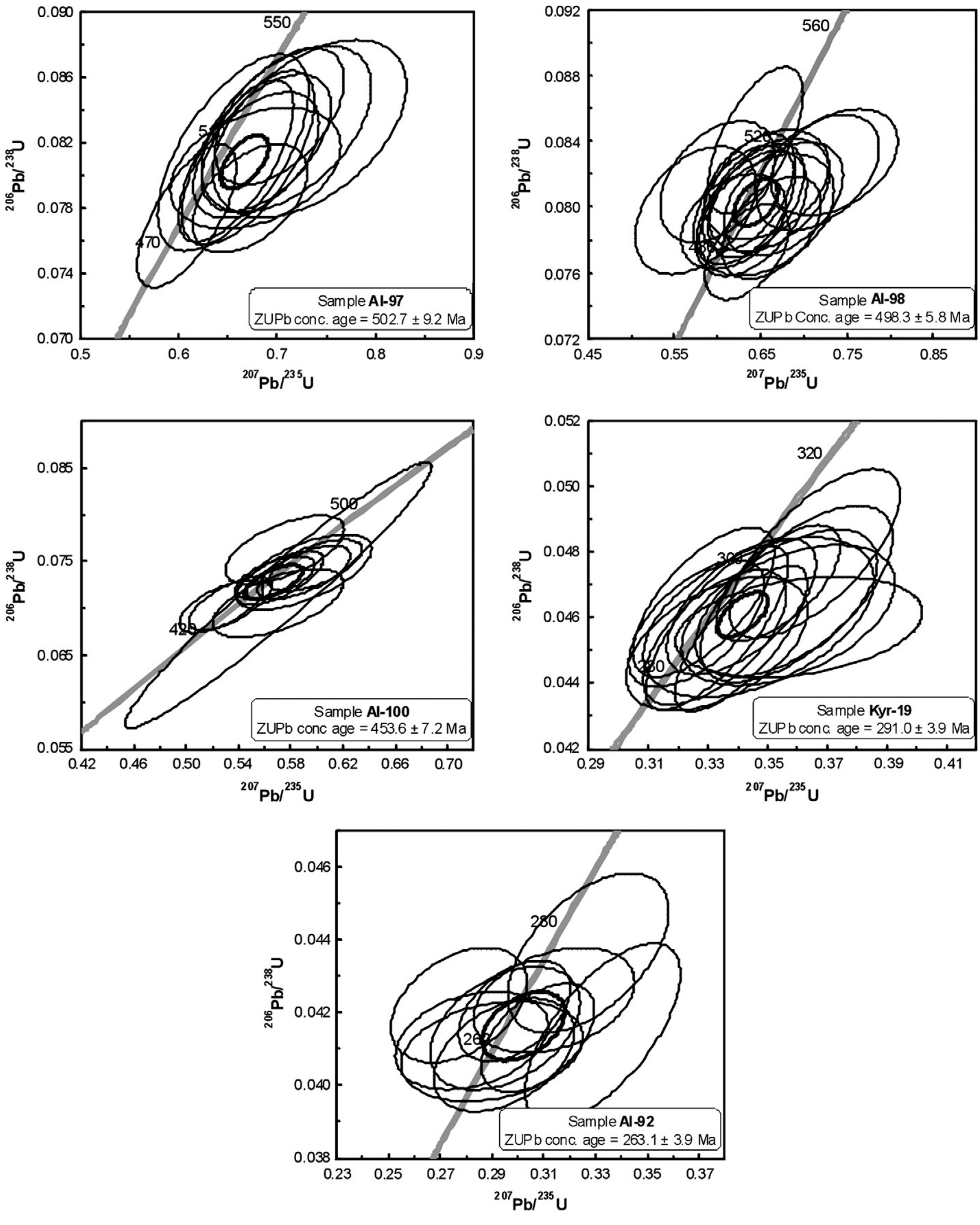

Fig. 4. Zircon U/Pb concordia plots for samples AI-92, AI-97, AI-98, AI-100 and KYR-19 (all concordant ages). Data point error ellipses are 2 σ, concordia age error is 95% confidence, decay errors included. MSWD values for all plots between about 1 and 4.

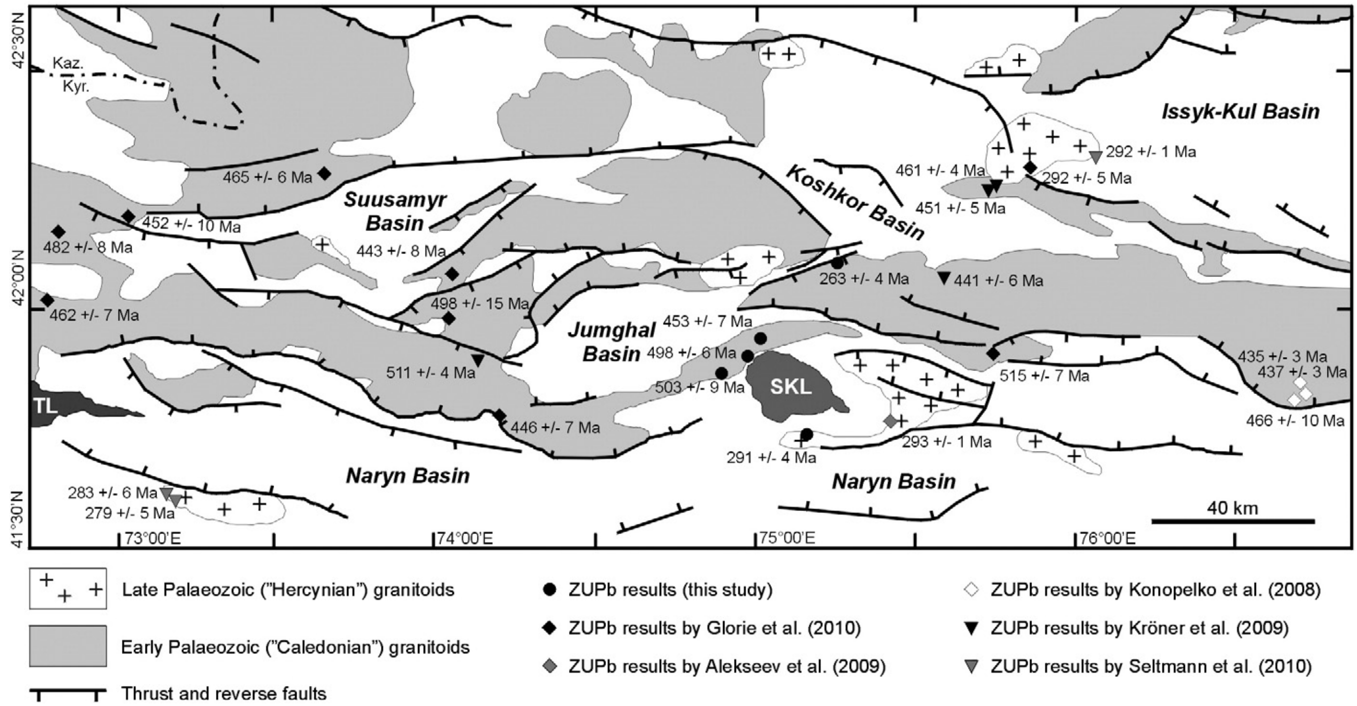

Fig. 5. Schematic geological map of the central section of the Northern and Middle Kyrgyz Tien Shan showing the plutonic rocks (Early and Late Palaeozoic granitoids) in this region. Zircon U/Pb (ZUPb) dating results from this and other studies (Konopelko et al., 2008; Alekseev et al., 2009; Kröner et al., 2009; Glorie et al., 2010a; Seltmann et al., in press) are indicated. See Fig. 1 for general location. SKL = Song-Kul Lake; TL = Toktogul Lake. Redrawn after Glorie et al. (2010a).

variation. All measured surfaces on the polished zircon grains were inclusion free. No inherited cores were observed for any of the samples. The 454 Ma age in general corresponds to similar ages obtained in the adjoining Suusamyrski complex by Glorie et al. (2010a) who report ages between about 440 and 450 Ma. The 503–498 Ma ages on the other hand corresponds to an age of 500 Ma reported in Mikolaichuk et al. (1997) from the same complex (Fig. 2). In any case, we interpret the ~503–498 Ma ZUPb age obtained for the Song-Kul-Too (quartz) diorites–tonalites to represent their crystallization age and therefore as the age of emplacement of a Late Cambrian island arc root.

It is not uncommon to find these Middle to Late Cambrian intrusion ages of ~515–498 Ma elsewhere along the Nikolaev Line (Fig. 5). The bulk of the "Caledonian" intrusions north of the Nikolaev Line however are in the 440–460 Ma age range and they represent the Late Ordovician–Early Silurian collision stage of the North Tien Shan micro-continent with palaeo-Kazakhstan and the development of an associated Andean type active margin (Konopelko et al., 2008; Gao et al., 2009; Biske and Seltmann, 2010). Although we were not able to confirm the emplacement age of the Suusamyrski complex in the Song-Kul area (samples AI-91 and AI-93) due to insufficient amounts of datable zircons, the complex typically yields Late Ordovician – Early Silurian ages at other locations more westward (e.g. Glorie et al., 2010a). As mentioned, the 453.6 ± 7.2 Ma age of sample AI-100 would fit well in this context, but no evidence was found to position AI-100 outside the "Cambrian" island arc complex. It should be noted that the Ordovician granitoids of the Suusamyrski complex were already exhumed by the onset of Early Permian subaerial volcanic activity. Early Permian volcanic rocks lie on top of an erosive contact on the granitoids (Fig. 2). In other places it can be shown that Middle–Early Carboniferous red beds and conglomerates overlie these granitoids as well. These observations are important thresholds used to constrain the thermal history models presented later in this paper.

Late Palaeozoic ZUPb ages are obtained for samples AI-92 and KYR-19. KYR-19, from the Song-Kul granitic massif (Bauralabas Range, south Song-Kul Basin, Fig. 2), gives an age of 291.0 ± 3.9 Ma (Early Permian, Sakmarian) and corresponds to a ZUPb age obtained by Alekseev et al. (2009) of 293 ± 1 Ma for the granites from the so-called third intrusion phase of the Song-Kul complex. The ZUPb age for AI-92, a lamprophyre dyke inside the granites of the Middle to Late Ordovician Terstorski complex, is 263.1 ± 3.9 Ma (Middle–Late Permian, Capitanian).

The emplacement age of ~291 Ma we found for the Song-Kul complex granites constrains the final collision of palaeo-Kazakhstan with the Tarim micro-continent. The collision corresponds to the terminal tectonic event responsible for the formation of the ancestral Tien Shan, wedged between Kazakhstan and Tarim. Alternatively, Seltmann et al. (in press) catalogue the Song-Kul complex as a "Hercynian" post-collisional granitoid intrusion. According to these authors, post-Hercynian magmatism occurs is a narrow time frame of ~295–280 Ma throughout the entire Tien Shan orogen, almost immediately following subduction related igneous activity at ~300–315 Ma.

The ZUPb age for the lamprophyre dyke in the Ordovician Terstorski complex is significantly younger at ~263 Ma. It would seem reasonable to associate this lamprophyre dyke with the Sandyk intrusion less than 10 km to the northwest of position AI-92. This is an alkaline Permian intrusion (mainly syenite and quartz syenite) with carbonatite zones (Jenchuraeva, 2001; Jenchuraeva et al., 2001; Tursungaziev and Petrov, 2008). If so, these intrusions are likely linked to a phase of post-collisional (post-Hercynian) Permian intraplate extension. Solomovich (2007) also reports on lamprophyre dykes ("vougnerites") associated with Permian alkaline post-collisional intrusions in the Kyrgyz Southern Tien Shan and De Grave et al. (in press) also date a felsic dyke in the STS (Alai area) to ~264 Ma. This shows that these dykes seem to occur in several places in the Kyrgyz Tien Shan, but solely based on the data from one dyke in this paper it would be hazardous to attach too much significance to this on a regional scale.

The post-collisional intrusions in several areas of the Kyrgyz Tien Shan have been extensively described and were dated for example at 279–299 Ma (Konopelko et al., 2007, 2009), 276–293 Ma (Seltmann et al., in press) and 292 Ma (Glorie et al., 2010a; Fig. 5). Similar ages

Table 5

TFT age data: n is the number of counted grains; ρ_s, ρ_i, and ρ_d are the density of spontaneous, induced tracks and induced tracks in an external detector (ED) irradiated against a dosimeter glass. The ρ_d-values are interpolated values from regularly spaced glass dosimeters (IRMM-540). ρ_d is expressed as 10^5 tracks/cm^2; ρ_s and ρ_i are expressed as 10^7 tracks/cm^2. N_s, N_i, and N_d are the number of counted spontaneous, induced tracks and induced tracks in the ED. N_d is an interpolated value. $P(\chi^2)$ is the chi-squared probability that the dated grains have a constant ρ_s/ρ_i-ratio. An ζ-value of 505.1 ± 7.8 a.cm^2 was used for the calculation of the TFT age t_ζ (in Ma, at 1σ). Absolute ages (Q-ages), t_Q, are listed as well to illustrate the compatibility of both calibration systems and to underscore the 'stable' observation efficiency of the tracks in titanite (OWMQ = 1.910 ± 0.070 based on Fish Canyon Tuff and Mount Dromedary titanite).

Sample	n	ρ_s (±1σ)	N_s	ρ_i (±1σ)	N_i	ρ_d (±1σ)	N_d	ρ_s/ρ_i	$P(\chi^2)$	t_ζ	t_Q
AI-99	14	2.163 (0.049)	1924	1.132 (0.036)	1003	4.026 (0.079)	2585	1.929 ± 0.214	0.72	193.2 ± 8.9	192.7 ± 11.0
KYR-16	2	1.963 (0.086)	515	1.006 (0.062)	263	3.995 (0.079)	2553	1.951 ± 0.148	0.81	193.9 ± 15.5	194.9 ± 15.3
KYR-18	17	2.354 (0.029)	6462	1.019 (0.019)	2841	3.999 (0.079)	2558	2.331 ± 0.052	0.11	231.2 ± 7.8	232.2 ± 11.0
KYR-19	22	0.928 (0.012)	5762	0.406 (0.080)	2546	4.004 (0.079)	2563	2.283 ± 0.054	0.10	226.8 ± 7.8	227.5 ± 10.9

are obtained in the Chinese part of the Tien Shan as well (e.g. Gao et al., 2009). In the Alai section (west of the Talas-Ferghana fault zone) of the Southern Kyrgyz Tien Shan we found somewhat younger ages between 264 and 284 Ma (De Grave et al., in press). Konopelko et al. (2007, 2009) and Seltmann et al. (in press) propose that large scale Permian post-orogenic deformation along strike-slip faults and shear zones in the Tien Shan orogen offered a suitable setting for the intrusion of these igneous complexes. The large strike-slip faults and shear zones provide potential conduits for the magmas that exhibit geochemical characteristic of a lithospheric mantle source contaminated with crustal components (e.g. Pirajno, 2010). Konopelko et al. (2007) further suggest a link between the alkaline post-Hercynian Tien Shan intrusions with alkaline igneous rocks in the Tarim Basin. Recently these igneous rocks in the Tarim Basin have been linked to the existence of a mantle plume and associated Permian flood basalts that seem to make up a Large Igneous Province (LIP), now for a large part buried underneath the thick Meso-Cenozoic Tarim Basin cover. Several rocks from the supposed LIP have been dated in recent years. Alkaline basalts were dated by $^{40}Ar/^{39}Ar$ and yield ages between 262 and 285 Ma (Zhang et al., 2010); associated rhyolites were dated by SHRIMP zircon U/Pb, yielding ages of 272 to 291 Ma (Tian et al., 2010); and a SHRIMP zircon U/Pb analysis on a quartz syenite from a layered intrusive complex gave ~274 Ma (Zhang et al., 2008).

3.2. Titanite fission-track dating

TFT ages are obtained for four samples and are all restricted to the Late Triassic (Carnian) and the Early Jurassic (Sinemurian): AI-99 (193.2 ± 8.9 Ma), KYR-16 (193.9 ± 15.5 Ma), KYR-18 (231.2 ± 7.8 Ma) and KYR-19 (226.8 ± 7.8 Ma). TFT ages and analytical details are reported in Table 5 and shown on Fig. 6. The ages were calculated both using absolute thermal neutron fluence calibration (t_Q) and zeta-calibration (t_ζ), and both calibration systems yield identical ages within analytical uncertainty. While AI-99 was sampled in the Late Cambrian Song-Kul-Too diorites, all other titanite samples come from the granites of the Early Permian Song-Kul igneous complex. As demonstrated previously by our data, the latter complex was emplaced at ~291 Ma. The post-magmatic cooling of the granite would most probably have occurred prior to the ~230 Ma TFT ages. TFT ages are cooling ages as titanites cool through the TFT partial annealing zone of ~265–310 °C (Coyle and Wagner, 1998). The TFT ages obtained here therefore represent a Late Triassic–Early Jurassic cooling event that seems to have affected the entire Song-Kul block, irrespective of basement lithology and age. This cooling event is also registered by the AFT thermochronometer as outlined below. We will first describe these AFT results and subsequently present the discussion and interpretation based on both the TFT and AFT data (including thermal history modeling).

3.3. Apatite fission-track dating and thermal history modeling

3.3.1. Apatite fission-track data

AFT ages (Table 6) obtained for the Song-Kul basement samples fall into three age clusters. As for TFT, the AFT ages are shown on the topographic cross-sections depicted in Fig. 6. Age–elevation relationships (TFT and AFT) are shown on Fig. 7. Track length data is presented in Fig. 8. The youngest age "cluster" in fact only contains the single sample AI-91. Its AFT age is 118.6 ± 5.4 Ma (Aptian; Early Cretaceous). The sample exhibits a Mean Track Length (MTL) of 12.56 µm (σ = 1.58 µm). A second cluster consists of samples AI-92 (154.3 ± 11.3 Ma), AI-93 (152.0 ± 10.8 Ma) and AI-98 (138.0 ± 5.7 Ma) and hence spans the latest Jurassic–earliest Cretaceous (Kimmeridgian–Valanginian). No AFT length information is available for AI-92 (due to an insignificant amount of confined tracks). MTL values for AI-93 and AI-98 are 12.61 µm (σ = 1.46 µm) and 13.20 µm (σ = 1.65 µm) respectively. All other samples can be grouped in a third cluster of Late Triassic–Early Jurassic (Norian–Toarcian) age, between 206.0 ± 13.9 Ma (KYR-17) and 182.5 ± 8.2 Ma (AI-102). Most MTL values for samples in this cluster range between ~12.8 and 13.8 µm (σ = ~1.2–1.6 µm). The samples from Bauralabas Range (KYR-16 and KYR-17) fall in this Late Triassic–Early Jurassic cluster, but their lengths are markedly shorter: 11.53 µm (σ = 1.61 µm) and 12.62 µm (σ = 1.13 µm) respectively.

3.3.2. Age-elevation relationships and the fossil Partial Annealing Zone

The age-elevation plot (Fig. 7) reveals a clear linear trend with increasing ages for increasing elevations. Both AFT and TFT ages are plotted on the graph. At around ~3050 m the AFT age-elevation plot exhibits a marked break-in-slope near the position of sample AI-102. Samples above the break-in-slope have AFT ages around ~190–200 Ma and describe a steep linear trend. Not much difference is noticed for the samples from the Song-Kul Range elevation profile (grey dots, full line) compared to the samples from the Bauralabas Range elevation profile (black dots, dashed line). Below the break-in-slope, samples have lower AFT ages (~120–180 Ma). This profile is typical for the upper section of an exhumed fossil Partial Annealing Zone (PAZ) that has not been eroded away significantly since its exhumation (e.g. Gleadow and Fitzgerald, 1987; Wagner and Van den haute, 1992; Fitzgerald and Stump, 1997). The PAZ of a FT system is a temperature window in which fission tracks are retained, but partially annealed, resulting in track shortening (Wagner and Van den haute, 1992 and references therein). In the case put forward here, sample AI-102 then more or less represents the position of the transition of the fossil retention zone (higher than AI-102) to the fossil PAZ (lower). The Late Triassic–Early Jurassic AFT ages (~183–206 Ma) above the break-in-slope therefore place minimal age constraints on the uplift-exhumation event that rapidly brought this basement from the

Fig. 6. Schematic topographic cross-sections across the Song-Kul Basin and bordering mountain ranges. Sample positions with their associated TFT, AFT and AHe ages are indicated (see Fig. 2 for location of cross-sections and Fig. 3 for a 3-D terrain view). Thermal history models obtained with HeFTy software (Ketcham, 2005) are added. For sample AI-91 good fit paths (dark grey) and acceptable fits (light grey) are depicted as a general illustration of typical thermal history modeling results for the Song-Kul samples. For other samples only good fit envelopes are drawn in order to keep the figure as comprehensible as possible. Time–temperature box constraints used for modeling are shown. See text for further details.

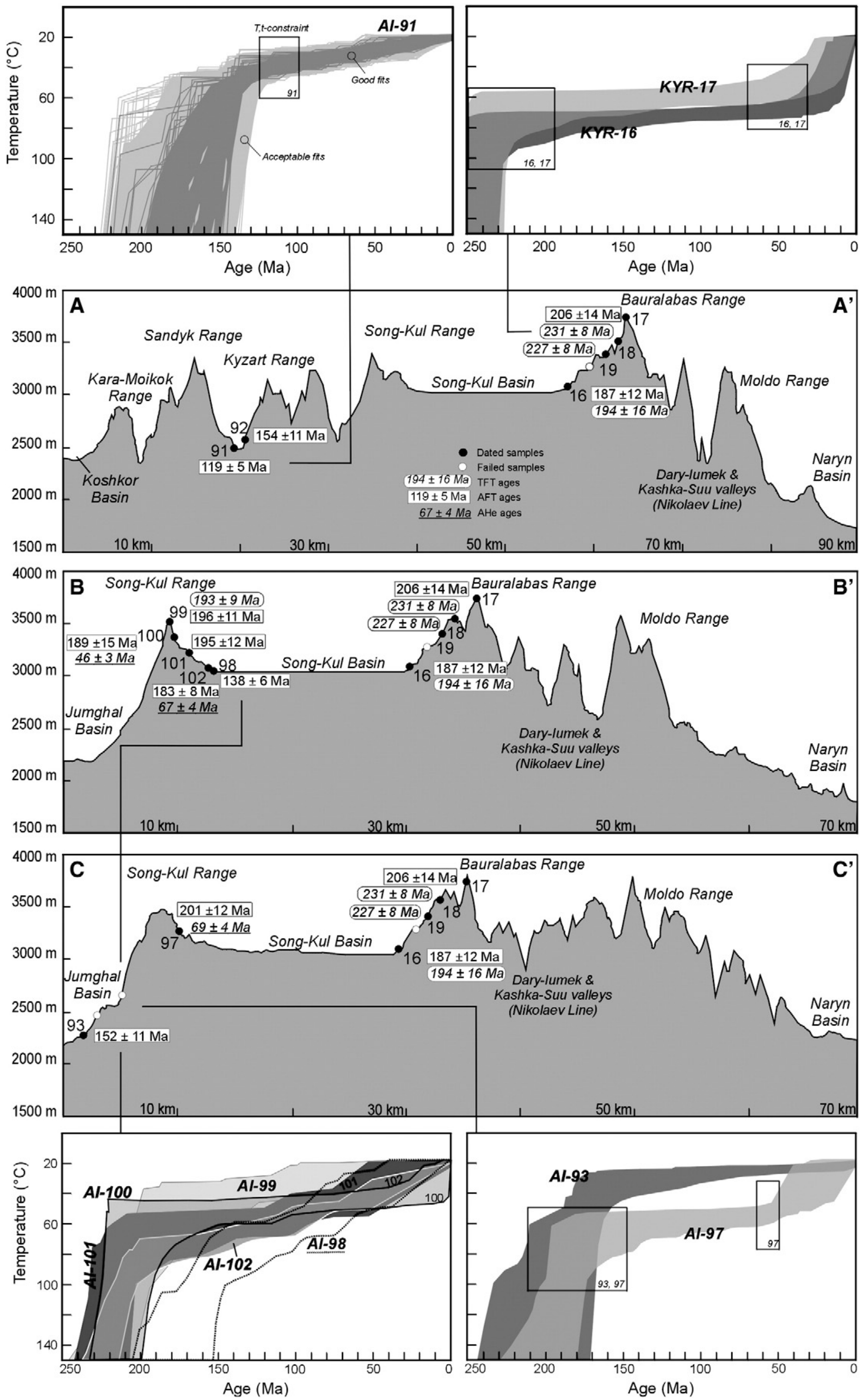

AI-91
T,t-constraint
Good fits
Acceptable fits
KYR-17
KYR-16
Temperature (°C)
Age (Ma)
A
A'
Sandyk Range
Kyzart Range
Kara-Moikok Range
Koshkor Basin
Song-Kul Range
Song-Kul Basin
Bauralabas Range
Moldo Range
Naryn Basin
Dary-lumek & Kashka-Suu valleys (Nikolaev Line)
206 ±14 Ma
231 ± 8 Ma
227 ± 8 Ma
187 ±12 Ma
194 ± 16 Ma
154 ±11 Ma
119 ± 5 Ma
Dated samples
Failed samples
TFT ages
AFT ages
AHe ages
67 ± 4 Ma
B
B'
Jumghal Basin
193 ± 9 Ma
196 ±11 Ma
195 ±12 Ma
189 ±15 Ma
46 ± 3 Ma
183 ± 8 Ma
138 ± 6 Ma
C
C'
201 ±12 Ma
69 ± 4 Ma
152 ± 11 Ma
AI-100
AI-99
AI-101
AI-102
AI-98
AI-93
AI-97

Table 6
AFT age and length data: n is the number of counted grains; ρ_s, ρ_i, and ρ_d are the density of spontaneous, induced tracks and induced tracks in an external detector (ED) irradiated against a dosimeter glass. The ρ_d-values are either interpolated values from regularly spaced glass dosimeters (IRMM-540) where irradiations showed axial gradients in thermal neutron fluence (irradiation batch with samples AI-98 and KYR-16 and batch with sample KYR-17), or an averaged value for irradiations where no gradient was detected (batch with rest of samples). ρ_d is expressed as 10^5 tracks/cm^2; ρ_s and ρ_i are expressed as 10^6 tracks/cm^2. N_s, N_i, and N_d are the number of counted spontaneous, induced tracks and induced tracks in the ED. N_d is an interpolated value where applicable, or otherwise an average. $P(\chi^2)$ is the chi-squared probability that the dated grains have a constant ρ_s/ρ_i-ratio. An ζ-value of 253.1 ± 2.4 a cm^2 was used for the calculation of the AFT age $t(\zeta)$ (in Ma, at 1σ). AFT length data are reported as a mean track length (l_m in μm) with standard deviation σ (in μm), obtained from the measurement of a number (n_l) of natural, horizontal confined tracks.

Sample	n	ρ_s ($\pm 1\sigma$)	N_s	ρ_i ($\pm 1\sigma$)	N_i	ρ_d ($\pm 1\sigma$)	N_d	ρ_s/ρ_i	$P(\chi^2)$	$t(\zeta)$	l_m	n_l	σ
AI-91	19	3.557 (0.078)	2084	1.536 (0.051)	906	3.773 (0.077)	2415	2.506 ± 0.100	0.17	118.6 ± 5.4	12.56	100	1.58
AI-92	18	4.082 (0.110)	1386	1.402 (0.066)	448	3.773 (0.077)	2415	3.270 ± 0.178	0.47	154.3 ± 11.3	-	-	-
AI-93	20	4.747 (0.121)	1539	1.556 (0.069)	512	3.773 (0.077)	2415	3.219 ± 0.164	0.30	152.0 ± 10.8	12.61	100	1.46
AI-97	20	1.245 (0.031)	1593	0.297 (0.015)	380	3.773 (0.077)	2415	4.279 ± 0.244	0.98	201.1 ± 12.3	13.01	100	1.30
AI-98	19	2.388 (0.044)	2904	0.829 (0.026)	1008	3.823 (0.077)	2447	2.940 ± 0.107	0.70	138.0 ± 5.7	13.20	100	1.65
AI-99	20	1.501 (0.034)	1921	0.368 (0.017)	471	3.773 (0.077)	2415	4.160 ± 0.214	0.91	195.6 ± 11.0	13.83	100	1.17
AI-100	15	0.832 (0.029)	799	0.216 (0.015)	207	3.773 (0.077)	2415	4.023 ± 0.314	0.99	189.3 ± 15.4	13.22	100	1.30
AI-101	30	1.467 (0.036)	1663	0.366 (0.018)	408	3.773 (0.077)	2415	4.144 ± 0.229	0.99	194.9 ± 11.6	13.09	100	1.42
AI-102	19	2.495 (0.023)	3193	0.662 (0.023)	847	3.773 (0.077)	2415	3.877 ± 0.150	0.62	182.5 ± 8.2	12.75	100	1.61
KYR-16	15	4.160 (0.121)	1187	1.266 (0.067)	354	4.211 (0.081)	2702	3.569 ± 0.216	0.11	187.4 ± 12.0	11.53	100	1.61
KYR-17	20	6.258 (0.165)	1442	1.336 (0.077)	305	3.353 (0.075)	2020	4.932 ± 0.071	0.81	206.0 ± 13.9	12.62	77	1.13

deeper crust, through the apatite PAZ. This event in other words was already taking place during the aforementioned age range. The AFT ages of the samples below the break-in-slope can hence be interpreted as mixed ages, between the Late Triassic–Early Jurassic event and a younger, post ~120–150 Ma event.

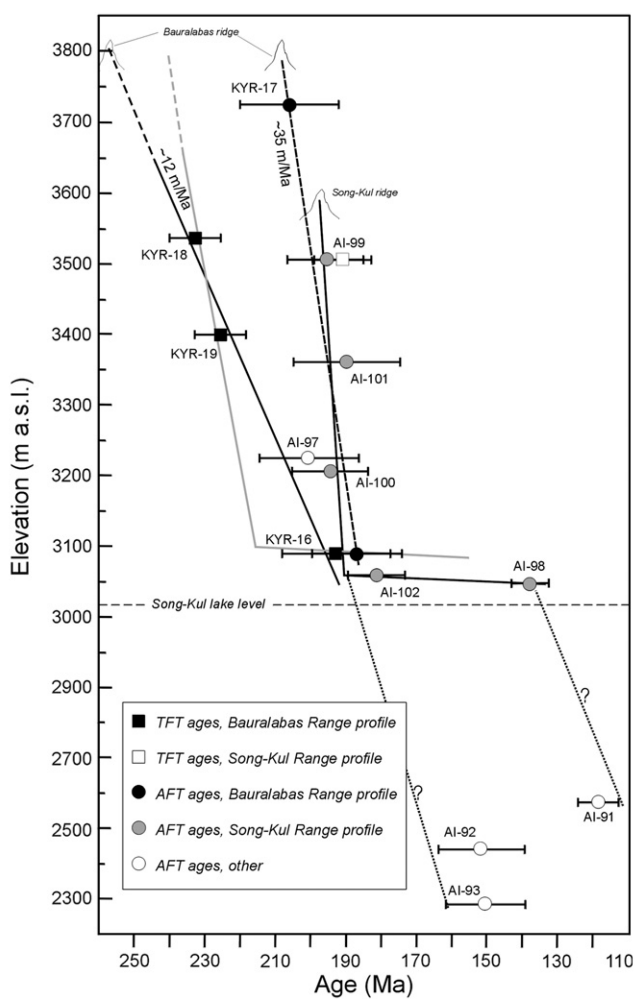

Fig. 7. AFT and TFT age-elevation plots for the Song-Kul Basin-vergent flanks of the Song-Kul (North) and Bauralabas (South) Ranges. The Song-Kul Lake level and the top ridges of both aforementioned mountain ranges are schematically shown. A break-in-slope in the AFT age-elevation plot is noticeable before sample AI-102 and after sample AI-98. It might also be present in the TFT profile (see text for discussion).

The TFT ages show that the Song-Kul basement was exhumed through the TFT PAZ just prior (~230–190 Ma) to the AFT PAZ (~183–206 Ma), suggesting a single, rapid and persisting Early Mesozoic uplift-exhumation episode in the Kyrgyz Tien Shan. This is also reflected in the thermal history models of the "above the break-in-slope" samples (Bauralabas Range profile, KYR samples and the Song-Kul Range Profile, AI-102–AI-98; Fig. 6). As mentioned previously the TFT PAZ is estimated at ~265–310 °C (Coyle and Wagner, 1998), while for apatite this temperature window is significantly lower from ~140–120 °C to 70–40 °C (Wagner and Van den haute, 1992 and references therein). In the case of apatite it should be mentioned that track retentivity and annealing additionally also depends on the chemical composition of the apatite (predominantly Clwt% and Cl/F ratio; e.g. Barbarand et al., 2003). When considering the TFT age of 193.9 ± 15.5 Ma (Table 5) and the AFT age of 187.4 ± 12.0 Ma (Table 6) of sample KYR-16, the exhumation through the titanite and subsequently through the apatite PAZ was indeed a rapid process, transpiring in about 6.5 million years. The ages for sample AI-99 (at higher elevation) even suggest a more rapid process. The calculated TFT age of this sample (193.2 ± 8.9 Ma) is slightly younger than the AFT age (195.6 ± 11.0 Ma) but can be considered identical within analytical uncertainty.

The AFT length data further underscore the observation of an exhumed fossil PAZ (Table 6, Fig. 8). MTL values for the samples above the fossil PAZ are relatively long (~13.0–13.8 μm), track length distributions are symmetric and narrow (σ = ~1.2–1.4 μm) in comparison to the samples in the fossil PAZ. The MTL values from the Bauralabas Range samples (KYR samples) are shorter (~11.5–12.6 μm) despite that their ages and age-elevation trends are very similar to those in the Song-Kul Range elevation profile (samples AI-99–AI-102; above the fossil PAZ). In their modeled thermal histories (Fig. 6) this is clearly reflected and the KYR samples stay at higher temperatures after Early Mesozoic cooling, followed by an additional (more moderate) Cenozoic cooling since the Eocene (~40–60 Ma). It should be noted that the apatites from the Bauralabas Range granites have lower D_{par} values than those from the Song-Kul Range diorites and tonalites. D_{par} is a so-called kinetic parameter that describes the annealing properties of a particular apatite and is positively correlated to the Clwt% (Cl/F content) of the apatite. D_{par} is the maximum etch pit diameter measured parallel to the crystallographic c-axis (e.g. Donelick et al., 2005). D_{par} also depends on the etching conditions applied for AFT revelation (Sobel and Seward, 2010). Given a certain etching condition, a higher D_{par} value is indicative of a higher Cl content of the apatite and hence of an apatite more resistant to annealing (e.g. Barbarand et al., 2003; Donelick et al., 2005). Or in other words, given a same set of annealing conditions, AFT lengths in a Cl-rich apatite will be longer that those of an apatite with less Cl in its lattice. In this case the lower D_{par} values of the apatites from the Bauralabas granite (KYR samples), implies a lower Cl content with respect to those from the Song-Kul Range. D_{par}'s were measured in at least 20 different grains, 5 measurements per grain. To illustrate this: sample KYR-16 has an average D_{par} of 1.61 ± 0.25 μm, compared to 2.59 ± 0.25 μm for sample AI-99 for example. As general bench mark: using our etching conditions we typically find D_{par} values for the Durango apatite standard ranging between ~1.5 and 1.9 μm (e.g. Glorie et al., 2010a). SEM analyses on c-axis parallel apatite sections revealed an average Cl content of 0.26 ± 0.09 wt.% for KYR-16, compared to 0.61 ± 0.17 wt.% for AI-99. A representative Durango apatite in our sample set gives a value of 0.32 ± 0.05 wt.% Cl. Consequently, the shorter lengths for sample KYR-16 and 17 are most likely attributed to a difference in chemical composition of the analyzed apatites. Moreover, sample KYR-16 might represent a sample that is already inside rather than above the fossil AFT PAZ. It then would define the approximate knick-point in the age-elevation plot as AI-102 seems to do for the Song-Kul Range samples. AI-102 and KYR-16 have more or less identical AFT ages of ~185 Ma, and the MTL value for KYR-16 (11.53 μm) is already significantly shorter than for KYR-17 (12.62 μm) at the top of the profile.

As mentioned, the AFT length data also points to an exhumed fossil PAZ. Increasing MTL values with increasing elevation on one hand, and decreasing standard deviation (SD) of the length–frequency distributions (i.e. more narrow distributions) with increasing elevation (Fig. 8) on the other hand, are a clear signature of an exhumed fossil PAZ. MTL versus AFT age and SD versus AFT age plots strengthen this point further (Fig. 8). These so-called boomerang plots exhibit longer lengths for older ages and more narrow distributions (smaller SD) for older ages (e.g. Green, 1986; Fitzgerald and Stump, 1997; Gallagher and Brown, 1997). In the case here, only “half boomerangs” are manifested in the data, because only the upper segment of the fossil PAZ is preserved and reflected in the data.

The TFT age-elevation plot of the Bauralabas samples (black squares, Fig. 7) is only defined by the three KYR (16, 18, 19) samples. The AI-99 TFT age does not seem to follow the trend. Two “end-member” situations can be plotted through this limited dataset: (1) a simple age-elevation profile with increasing ages for increasing elevation (black line), and (2) a profile with break-in-slope at an elevation of ~3100 m. Admittedly, the latter profile can only be inferred when considering the AFT age-elevation profile. When doing so, the AFT- and TFT “break-in-slope profile” are parallel and offset. The offset to higher elevations and ages of the TFT profile is to be expected bearing in mind the higher “closure temperature” of the TFT thermochronometer in comparison to the AFT thermochronometer. The configuration of the break-in-slope profiles in Fig. 7 is then very comparable to the typical configurations of chronometers with different closure temperatures (e.g. Stockli et al., 2000).

When taking into account the TFT age-elevation plot without break in slope (black full line, Fig. 7) and comparing it to the AFT age-elevation plot, e.g. to the Bauralabas Range samples (KYR samples, dashed line), a marked difference in slope is observed. When calculating an exhumation rate based on the TFT profile slope, a value of ~12 m/Ma is obtained. Based on the AFT profile slope on the same samples a threefold higher value of ~35 m/Ma is determined (Fig. 7). This is however not surprising. It is well-documented that age-elevation relationships based on thermochronological data can be significantly perturbed by topography (e.g. Huntington et al., 2007; van der Beek et al., 2010). In areas with rapid exhumation (as the Mesozoic Tien Shan), heat advection towards the surface compresses the lower-temperature isotherms at shallower depths. This effect is smoothed out when moving deeper, to higher-temperature isotherms (e.g. Braun, 2002). As a consequence low-temperature thermochronometers such as AHe and AFT tend to overestimate the exhumation rates as the upper part of an eroding rock column seems to move faster with respect to the (compressed) low-temperature isotherms, and the lower part of the same rock column seems to move slower. In other words, when drawing a the TFT age-elevation profile for the Bauralabas Range samples without break in slope, the more moderate slope thus obtained with relation to the AFT data would more reliably estimate exhumation rates, whilst the AFT profile would overestimate exhumation rates.

3.3.3. The Early Mesozoic cooling event and the Song-Kul basin

Late Triassic–Early Jurassic AFT ages are found throughout the entire Tien Shan (NTS, MTS, STS; and both in the Kyrgyz and Chinese parts) indicating that the Early Mesozoic event affected the entire ancestral Tien Shan orogen. For example, we report an AFT age of ~223 Ma in the Alai section of the STS (west of the Talas-Ferghana fault zone, on the southern edge of the Ferghana Basin) and an age of ~207 Ma in the Trans-Alai Range, at the Tien Shan–Pamir convergence zone (De Grave et al., in press). However, these latter results as well as the Late Triassic and earliest Jurassic ages reported for other localities in the Tien Shan (e.g. Bullen et al., 2001; Dumitru et al., 2001; Sobel et al., 2006b), are hitherto only found in the detrital apatite archive. The rocks that record the Early Mesozoic basement cooling event therefore seem to have been eroded away to a large extent during subsequent, younger denudation events. Apparently only in very distinct and “protected” localities, does this AFT age population show up in the Tien Shan basement rocks. To the best of our knowledge, the results from the Song-Kul region presented here, represent the first report of a clear Late Triassic–Early Jurassic (~210–190 Ma) cooling event preserved in the AFT system of Tien Shan basement rocks. More specifically, the Song-Kul samples that reveal this event are exclusively found on the basin-vergent flanks (Song-Kul Range and Bauralabas Range). It seems reasonable to explain this by the hypothesis that the current morphology of the basin (Fig. 3) was already established in the Early Mesozoic to some extent. In this model, the Song-Kul basement rocks were exhumed to the (near) surface at the cessation of the Late Triassic–Early Jurassic event. The Song-Kul Basin would have developed subsequently as a largely internally drained basin, protected by mountain ranges that envelop the basin almost completely. Erosion and denudation strongly affect the external rim of the Song-Kul block, while the internal, basin-vergent flanks of the surrounding ranges would only experience minor effects, allowing them to preserve the fossil, Early Mesozoic upper AFT PAZ signature as described above. This process is well-known for large internally drained contractional basins such as on the Tibetan Plateau, the Andean Altiplano and the Tarim Basin for example (e.g. Sobel et al., 2003).

From the Middle and Late Triassic, lasting until the Early Jurassic, the Palaeo-Tethys Ocean was subducting underneath the southern active margin of Eurasia and eventually the peri-Gondwanan or Cimmerian fragment of Qiangtang collided with that margin. This collision occurred between ~200 and 230 Ma, along the Jinsha suture in what is now Central Tibet, and can be traced to the current northern Pamir Mountains (e.g. Schwab et al., 2004). The timing of this tectonic event coincides well with the TFT ages from this study and with the AFT ages from the “upper fossil PAZ” samples and their thermal history models (Fig. 6 and 9). Similar AFT ages, but then exclusively from the detrital record, have been linked to this event (e.g. Bullen et al., 2001; Dumitru et al., 2001; Sobel et al., 2006b; De Grave et al., in press). Indeed, the Qiangtang collision induced a period of tectonic reactivation (Cimmerian orogeny) in the Mesozoic Tien Shan orogen as evidenced by structural geological and sedimentological data (e.g. Graham et al., 1993; Allen et al., 1995; Otto, 1997; Allen and Vincent, 1997; Hendrix, 2000; Vincent and Allen, 2001). We interpret the Late Triassic–Early Jurassic AFT ages in the Song-Kul basement as cooling ages related to denudation–exhumation of this basement block during tectonic reactivation of the Tien Shan as response to the Qiangtang collision.

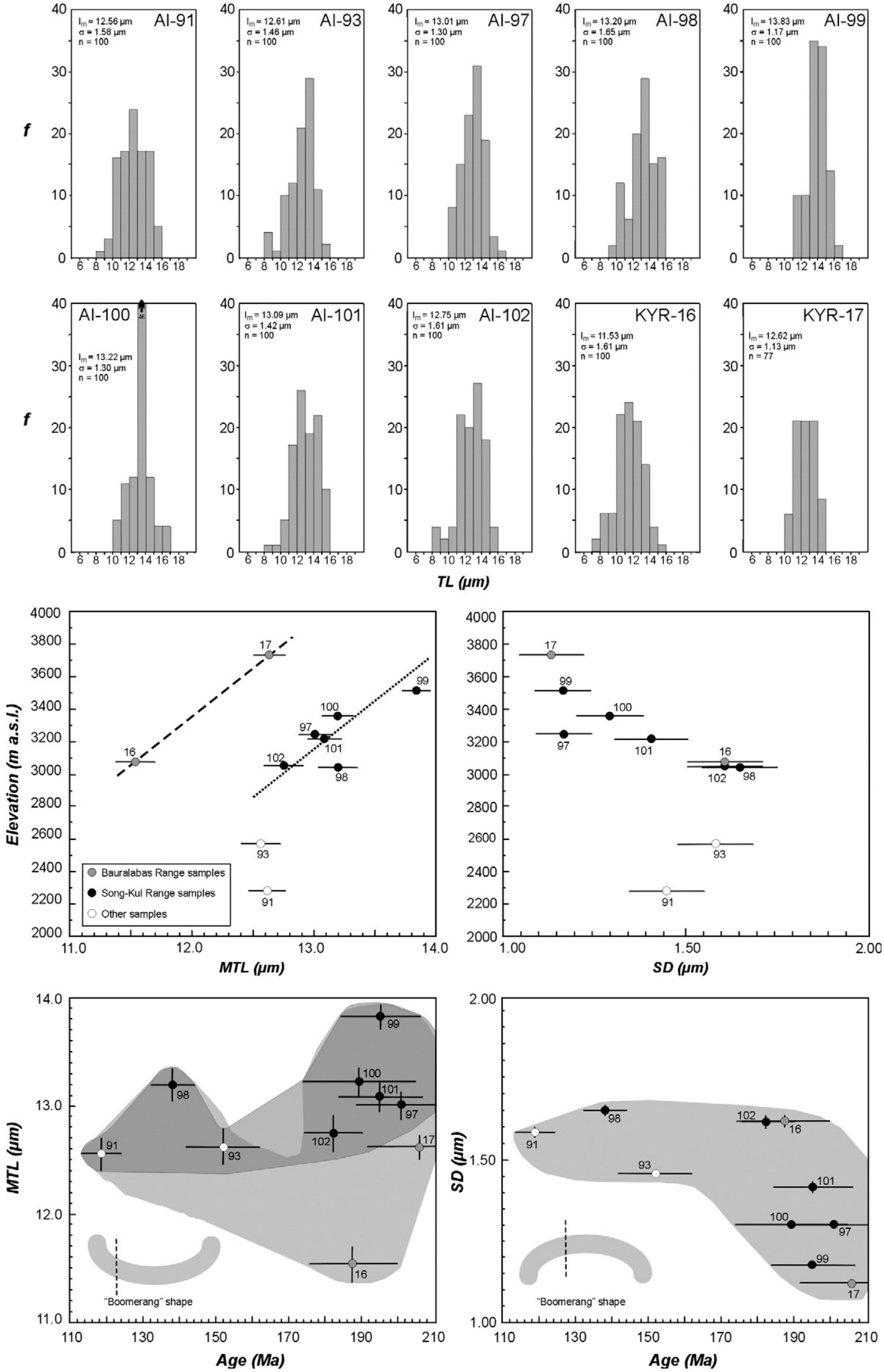
AI-91
lm = 12.56 µm
σ = 1.58 µm
n = 100
AI-93
lm = 12.61 µm
σ = 1.46 µm
n = 100
AI-97
lm = 13.01 µm
σ = 1.30 µm
n = 100
AI-98
lm = 13.20 µm
σ = 1.65 µm
n = 100
AI-99
lm = 13.83 µm
σ = 1.17 µm
n = 100
AI-100
lm = 13.22 µm
σ = 1.30 µm
n = 100
AI-101
lm = 13.09 µm
σ = 1.42 µm
n = 100
AI-102
lm = 12.75 µm
σ = 1.61 µm
n = 100
KYR-16
lm = 11.53 µm
σ = 1.61 µm
n = 100
KYR-17
lm = 12.62 µm
σ = 1.13 µm
n = 77
f
TL (µm)
Elevation (m a.s.l.)
MTL (µm)
SD (µm)
Bauralabas Range samples
Song-Kul Range samples
Other samples
"Boomerang" shape
MTL (µm)
SD (µm)
Age (Ma)
Age (Ma)

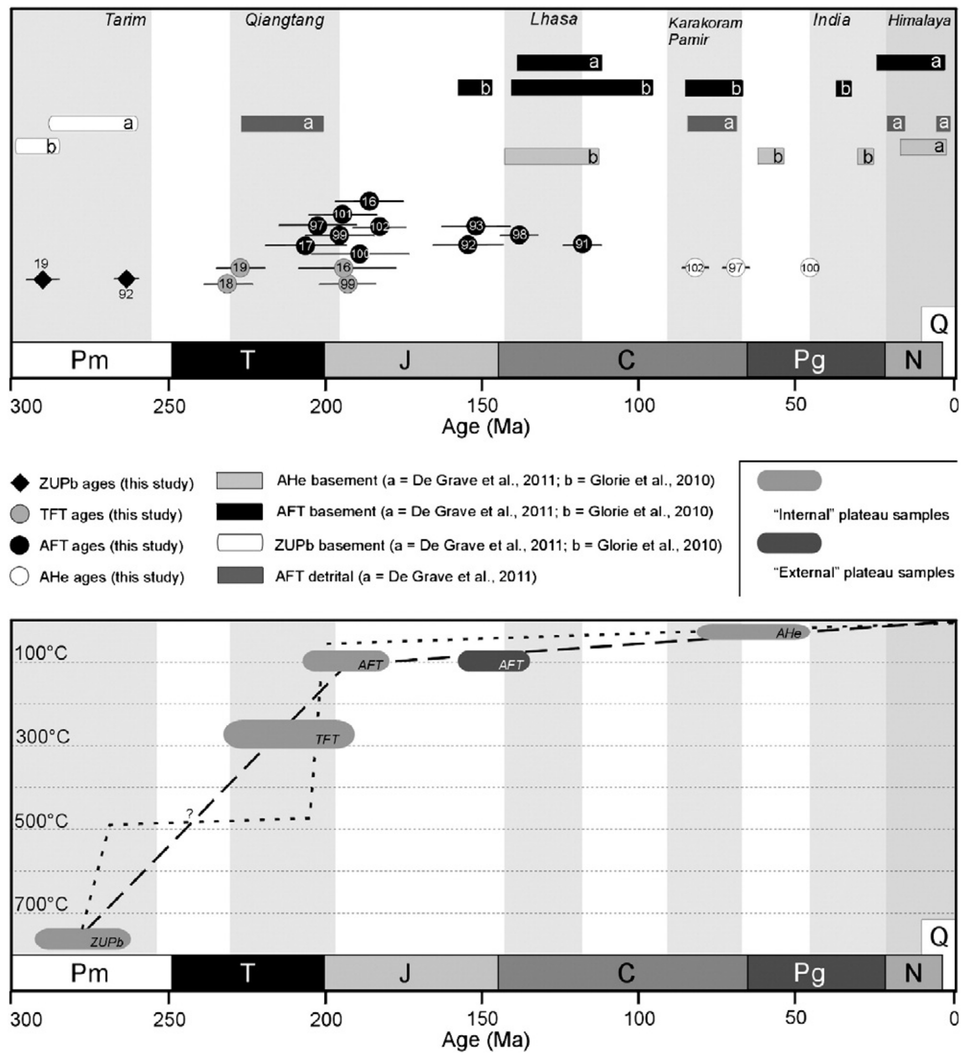

Fig. 9. Top panel: tectonic events associated to the ages obtained for the Northern Kyrgyz Tien Shan Song-Kul samples from multi-method geochronology and thermochronology. The obtained ages are compared against similar results (age ranges given) from previous studies in the Northern and Middle (Glorie et al., 2010a) and the Southern Kyrgyz Tien Shan (De Grave et al., in press). Results from samples for this study are shown individually and they are labelled with their associated "number" (i.e. "91" for AI-91, "16" for KYR-16 and so on). Bottom panel: schematic cooling path of the Song-Kul basement samples through time as derived from the obtained (multi-method) ages. See text for discussion.

3.3.4. The post-Early Mesozoic evolution

Following the Late Triassic–Early Jurassic episode, the Tien Shan was subjected to two additional pulses of reactivation, both also linked to the closure of the Tethyan Ocean and the ensuing pulses of the Cimmerian orogeny. The Lhasa (along the Bangong–Nujiang suture) and the Dras-Kohistan-Ladakh (along the Shyok suture) blocks were amalgamated to southern Eurasia in the Early and Late Cretaceous respectively (e.g. Schwab et al., 2004 and references therein). After cessation of the protracted Mesozoic tectonic episodes, a Late Cretaceous–Early Palaeogene erosional surface or peneplain developed in the Tien Shan region. This surface was subsequently deformed and tilted during the Late Cenozoic building of the modern Tien Shan (Burbank et al., 1999; Sobel et al., 2006a) as a far-field effect of India–Eurasia convergence. These events all had their influence on the formation and shaping of the current Tien Shan orogen and are recognized in both its detrital and basement thermochronological record (e.g. Bullen et al., 2001; Dumitru et al., 2001; Sobel et al., 2006b; Glorie et al., 2010a; De Grave et al., in press). However in the Song-Kul area their influence was limited and post-Early Mesozoic denudation was clearly insufficient to erode the Late Triassic–Early Jurassic exhumed fossil PAZ. This is further supported by the fact that well-preserved Mesozoic peneplanation surfaces occur south of Song-Kul, in the Moldo Range. However, the samples at the external margins of the Song-Kul block (Figs. 2, 3, 6), e.g. AI-91, 92 and 93 yield Late Jurassic–Early Cretaceous ages that either represent samples that were exhumed during the Lhasa collision induced reactivation, or simply represent a mixed age of incomplete reset samples from within the exhumed fossil PAZ. Their exhumation might then have been the combined denudational result of the Late Mesozoic and Late Cenozoic reactivation events. In any case, the samples at the external margins of the Song-Kul block represent deeper incised basement with respect to the internal part. The latter remained "protected" from the more recent events as the Song-Kul Basin developed into an internally drained plateau-like morphological feature at the border zone between the Northern and Middle Kyrgyz Tien Shan. The fact that Song-Kul is situated along or even within the important Nikolaev Line structure might be related to this observation. Therefore the post-Early Mesozoic deformation that affected large areas of the Tien

Fig. 8. Top: Track length–frequency (TL–f) distributions obtained from the AFT data of the Song-Kul samples; l_m = mean track length, with standard deviation (σ); n = number of measured horizontal confined tracks. Middle: Mean Track Length (MTL) and standard deviation (SD) versus elevation plots. Bottom: "Boomerang plots" (Green, 1986) of AFT age versus MTL and versus SD. See text for discussion.

Table 7
Apatite (U–Th–Sm)/He dating results. Aqt = Aliquot number. Concentrations for U, Th and Sm are listed in ppm, the ^{4}He concentration is in nmol/µg. The mass, m, of the apatite grains is in µg. F_T is the α-ejection correction factor (Farley, 2002; Farley et al., 1996). Single grain ages for each aliquot are given, and an average sample value is calculated (1σ). For comparison, AFT ages are listed as well.

Sample	Aqt	U	Th	Sm	Th/U	He	m	F_T	Age	Average	AFT age
AI-91	1	6.7	10.4	36.2	1.5	6.38	4.1	0.72	172.9 ± 10.4		
	2	31.9	87.0	22.8	2.7	36.18	5.1	0.73	171.8 ± 10.3		
	3	4.2	75.5	50.7	18.0	16.00	4.3	0.71	184.8 ± 11.1	176.5 ± 10.6	118.6 ± 5.4
AI-97	1	7.7	1.9	17.5	0.2	2.47	13.0	0.81	67.7 ± 4.1		
	2	7.5	1.3	16.5	0.2	2.30	4.7	0.75	71.6 ± 4.3		
	3	9.2	5.0	34.7	0.5	2.79	4.0	0.72	67.0 ± 4.0	68.8 ± 4.1	201.1 ± 12.3
AI-100	1	6.5	1.0	13.9	0.2	1.08	7.6	0.79	37.1 ± 2.2		
	2	8.6	3.2	32.4	0.4	2.01	1.7	0.64	*60.6 ± 3.6*		
	3	10.3	2.5	18.8	0.2	1.59	2.4	0.68	38.9 ± 2.3	45.5 ± 2.7	189.3 ± 15.4
AI-102	1	5.6	4.2	11.5	0.7	1.70	10.5	0.80	58.6 ± 3.5		
	2	23.2	10.2	18.6	0.4	8.51	14.1	0.82	74.9 ± 4.5		
	3	15.9	21.2	22.3	1.3	8.88	7.7	0.77	101.3 ± 6.1	78.3 ± 4.7	182.5 ± 8.2

Shan, in the Song-Kul area is probably largely accommodated along the bordering Nikolaev structure. From offsets along the Nikolaev Line, a non-negligent amount of post-Permian sinistral displacement can be deduced (Jenchuraeva, 2001; Solomovich, 2007; Tursungaziev and Petrov, 2008; Alekseev et al., 2009). Our data suggests that if Late Mesozoic and/or Late Cenozoic deformation was to an important degree partitioned as sinistral shear along the Nikolaev Line, the Song-Kul area behaves as a protected MTS fault block in the shear zone atop of which the Song-Kul Basin could develop. This implies that the current morphology of the Song-Kul area was already shaped to a large degree immediately succeeding the Late Triassic–Early Jurassic event. Its later evolution did not greatly affect the internal drainage pattern of the basin. The Song-Kul block did experience uplift from lower elevations at the end of the Mesozoic to its present alpine conditions. The block was hence uplifted to a relatively unbroken, high mountain plateau where rock uplift and surface uplift are virtually identical. Only at the rims of the uplifted plateau did erosion/denudation incise the basement to deeper levels.

To the southwest of the current Song-Kul Basin, in the Kara-Kichi and Min-Kush valleys, important Jurassic coal-bearing continental sediments (from low-lying lagoonal environments) unconformably cover Carboniferous sediments (Figs. 2 and 3). Kara-Kichi and Min-Kush represent a vital coal-mining district in the Kyrgyz Tien Shan. In the larger intramontane basins (e.g. Ferghana Basin, Issyk-Kul Basin and others) similar sediments occur and reach thicknesses of several hundred meters to more than 1 km. In the foreland basins to the Tien Shan (Junggar, Tarim), Early Mesozoic sedimentary deposits of over 3 to 4 km thick are present (e.g. Hendrix, 2000). These deposits can be associated with the erosion of the Late Triassic–Early Jurassic Tien Shan orogen.

3.4. Apatite (U–Th–Sm)/He thermochronometry

The AHe ages are listed in Table 7 and shown on the cross-section in Fig. 6. Thermal history models (HeFTy software; Ketcham, 2005) for samples AI-97, AI-100 and AI-102 (Fig. 6) were constructed based on both the available AFT data and the AHe ages. The AHe ages for the samples mentioned here were found to be Late Cretaceous–Early Palaeogene (~78–46 Ma). This corresponds to a period of tectonic quiescence and the development of a characteristic peneplanation surface across the entire Tien Shan area as outlined above. For sample AI-97 (average 68.8 ± 4.1 Ma) reproducibility of the ages for all three single grain aliquots was excellent. For AI-100 (average 45.5 ± 2.7 Ma) two aliquots produce an age of 38.0 ± 2.3 Ma, while one outlier of ~61 Ma is observed. The grain in this latter aliquot is somewhat smaller than the others, but based on the chemical properties (Table 7) there is no immediate reason to reject this analysis. The He-content for this "older" aliquot is higher and some minor, undetected inclusions might have been present in this grain, resulting is excess, parentless ^{4}He. It was opted not to reject the ~61 Ma age. The overall age average of the three aliquots of 45.5 ± 2.7 Ma does not differ substantially from the average of 38.0 ± 2.3 Ma when we only consider aliquots 1 and 3 from sample AI-100 (Table 7). Moreover, we interpret the AHe ages from the Song-Kul area as cooling ages related to slow cooling, slow denudation of the basement over a long Late Mesozoic–Cenozoic period, in a "protected" internally drained basin as explained in the previous sections. Therefore they are not related to a distinct orogenic phase for example. The AHe age is used here merely as a low-temperature constraint in the thermal history modeling procedure. The aliquots from sample AI-102 on the other hand all yield different ages, ranging from 101 to 59 Ma. There is no definite argument to favour one specific aliquot and reject another. The age variation is still constrained to the general Late Cretaceous–Early Palaeogene period described by the AHe ages of the three aforementioned samples. Therefore we opted to retain the average 78.3 ± 4.7 Ma average of the triplicate analysis for the input to the thermal history modeling.

While samples AI-97, 100 and 102 are from the "internal", basin-vergent mountain range flanks of the Song-Kul Basin, AI-91 is from the "external" part. The AHe results for AI-91 are more problematic. The three aliquots for this sample point toward a good reproducibility, however the reproducible average AHe age of 176.5 ± 10.6 Ma is not in agreement with the AFT age of 118.6 ± 5.4 Ma. As the AHe system is characterized by a lower "closure temperature" than the AFT system, one expects younger AHe age with respect to the AFT ages in a single sample. This is clearly not the case for sample AI-91. Anomalously high AHe ages with respect to AFT ages constitute a well-known problem (e.g. Green and Duddy, 2006; Spiegel et al., 2009) and are often attributed to either excess ^{4}He produced by inclusions, to radiation damage and He-trapping (Shuster et al., 2006) or to ^{4}He implantation from adjacent U-rich minerals and rocks (Spiegel et al., 2009). Given the fact that it is only sample AI-91 that shows this effect, and that all three aliquots produce nice reproducible ages, it is not clear what the cause of the anomalously high AHe age might be in this particular case. It was therefore decided not to include the AI-91 AHe age in the discussion and it was indeed not possible to perform thermal history modeling on the AHe and AFT input of sample AI-91. The modeled thermal history of this sample (Fig. 6) was therefore obtained by sole AFT input.

4. General model and conclusions

The Late Palaeozoic to Cenozoic ages for the Song-Kul samples obtained from the various methods applied here are shown in overview on Fig. 9. The ages are presented here in comparison with those obtained from other studies and within a general tectonic–geodynamic framework. Collision accretion events (e.g. Tarim, Qiangtang and others) that affected the Tien Shan orogen are schematically indicated. The Early Palaeozoic ZUPb ages obtained on the Song-Kul-Too diorite complex are not included in this figure.

The following conclusions could be drawn:

(1) ZUPb dating of the Song-Kul-Too diorite–tonalite complex of the northern Song-Kul igneous basement yielded a Late Cambrian emplacement age of ~498–502 Ma. These intrusive rocks are thought to represent the root of an ancient island arc system that accreted to the Northern Kyrgyz Tien Shan micro-continent in the Early Ordovician.

(2) The main and terminal intrusion phase (predominantly of granitic and granodioritic composition) of the Song-Kul igneous complex was dated to the Early Permian, with a ZUPb emplacement age of ~291 Ma. At that time, the southern rim of the Northern and Middle Kyrgyz Tien Shan, including the Song-Kul area, was involved in the collision–accretion zone of the Tarim micro-continent with palaeo-Kazakhstan of which the Northern Tien Shan already was a composing unit.

(3) A biotite-bearing lamprophyre dyke north of the Song-Kul basement is Possibly associated with an alkaline (syenite with carbonatite) post-collisional pluton. The ZUPb age of the dyke was established as 263 Ma, placing its intrusion to the Late Permian.

(4) Titanite fission-track (TFT) ages from the Song-Kul intrusive complex in the southern bordering Bauralabas Range and from the Song-Kul-Too diorites in the northern Song-Kul Range, give Middle to Late Triassic ages of ~193–231 Ma.

(5) Apatite fission-track (AFT) basement ages from this area yield Late Triassic–Early Jurassic ages of ~183–206 Ma. Thermal history modeling revealed a rapid Late Triassic–Early Jurassic cooling event affecting the Song-Kul basement. We interpret the TFT and AFT ages and the tT cooling paths revealed by the thermal history models in terms of exhumation of the Song-Kul basement during a period of tectonic reactivation. This tectonic reactivation is linked to the closure of the Palaeo-Tethys Ocean and collision of the Qiangtang terrane with the active southern Eurasian margin between ~190 and 230 Ma. The TFT and AFT ages are the first thermochronological constraints on this event preserved in Tien Shan basement rocks, in contrast to previously reported detrital cooling ages.

(6) Post-Early Mesozoic denudation of the Song-Kul basement was limited. This is attested by the fact that the upper section of an exhumed fossil AFT partial annealing zone (PAZ) is preserved in the basin-vergent mountain range flanks enclosing the Song-Kul basement. AFT length data corroborate this observation. Although based on limited data, a possible uplifted TFT PAZ might also be preserved. Post-Early Mesozoic denudation on the other hand did affect the outer rims of the Song-Kul block. The current morphology of the Song-Kul block was already established after the Early Mesozoic event. Late Mesozoic–Cenozoic reactivation of the Tien Shan produced uplift of the block to its present position, without exerting significant denudation. The Song-Kul Basin thus developed into an internally drained alpine plateau.

(7) Apatite (U–Th–Sm)/He (AHe) ages also point toward a slow terminal cooling of the basement to current conditions. Late Cretaceous–Palaeogene AHe ages ranging between ~46 and 78 Ma are not linked to a single tectonic event, but are rather translated to slow terminal exhumation through the AHe partial retention zone from the Late Mesozoic to the present.

Acknowledgements

The authors are supported by grants of the Fund for Scientific Research—Flanders (FWO, Belgium) (JDG) and the Institute for the Promotion of Innovation through Science and Technology in Flanders (IWT-Vlaanderen) (SG). This research was also co-funded by Ghent University (BOF—bilateral project 01SB1309). We are indebted to Dr. Guido Vittiglio and Dr. Peter Vermaercke for help with irradiations and neutron dosimetry at the Belgian Nuclear Research Centre in Mol (SCK-CEN, BR1 facility). We are very grateful to Dr. Daniel F. Stockli from Kansas State University for the apatite He analyses. Dr. Dmitry Konopelko and an anonymous reviewer are acknowledged for their critical comments that undoubtedly contributed to this paper.

References

Alekseev, D.V., Aristov, V.A., Degtyarev, K.E., 2007. The age and tectonic setting of volcanic and cherty sequences in the ophiolite complex of the Atbashe Ridge (Southern Tien Shan). Doklady Earth Sciences 413, 380–383.

Alekseev, D.V., Degtyarev, K.E., Kotov, A.B., Sal'nikova, E.B., Tret'yakov, A.A., Yakovleva, S.Z., Anisimova, I.V., Shatagin, K.N., 2009. Late Paleozoic subductional and collisional igneous complexes in the Naryn Segment of the Middle Tien Shan (Kyrgyzstan). Doklady Earth Sciences 427, 760–763.

Allen, M.B., Vincent, S.J., 1997. Fault reactivation in the Junggar region, northwest China: the role of basement structures during Mesozoic–Cenozoic compression. Journal of the Geological Society of London 154, 151–155.

Allen, M.B., Şengör, A.M.C., Natal'in, B.A., 1995. Junggar, Turfan and Alakol basins as Late Permian to ?Early Triassic extensional structures in a sinistral shear zone in the Altaid orogenic collage, Central Asia. Journal of the Geological Society of London 152, 327–338.

Barbarand, J., Carter, A., Wood, I., Hurford, A.J., 2003. Compositional and structural control of fission-track annealing in apatite. Chemical Geology 198, 107–137.

Biske, Yu.S., Seltmann, R., 2010. Paleozoic Tian-Shan as a transitional region between the Rheic and Urals–Turkestan oceans. Gondwana Research 17, 602–613.

Blackburn, T.J., Stockli, D.F., Carlson, R.W., Berendsen, P., 2008. (U–Th)/He dating of kimberlites—a case study from north-eastern Kansas. Earth and Planetary Science Letters 275, 111–120.

Braun, J., 2002. Quantifying the effect of recent relief changes on age–elevation relationships. Earth and Planetary Science Letters 200, 331–343.

Bullen, M.E., Burbank, D.W., Garver, J.I., Abdrakhmatov, K.Ye., 2001. Late Cenozoic tectonic evolution of the northwestern Tien Shan: new age estimates for the initiation of mountain building. Geological Society of America Bulletin 113, 1544–1559.

Burbank, D.W., McLean, J.K., Bullen, M., Abdrakhmatov, K.Y., Miller, M.M., 1999. Partitioning of intramontane basins by thrust related folding, Tien Shan, Kyrgyzstan. Basin Research 11, 75–92.

Coyle, D.A., Wagner, G.A., 1998. Positioning the titanite fission-track partial annealing zone. Chemical Geology 149, 117–125.

De Corte, F., Bellemans, F., Van den haute, P., Ingelbrecht, C., Nicholl, C., 1998. A new U doped glass certified by the European Commission for the calibration of fission-track dating. In: Van den haute, P., De Corte, F. (Eds.), Advances in fission-track geochronology. Kluwer Academic Publishers, Dordrecht, pp. 67–78.

De Grave, J., Van den haute, P., 2002. Denudation and cooling of the Lake Teletskoye region in the Altai Mountains (South Siberia) as revealed by apatite fission-track thermochronology. Tectonophysics 349, 145–159.

De Grave, J., Buslov, M.M., Van den haute, P., 2007. Distant effects of India–Eurasia convergence and Mesozoic intracontinental deformation in Central Asia: constraints from apatite fission-track thermochronology. Journal of Asian Earth Sciences 29, 188–204.

De Grave, J., Van den haute, P., Buslov, M.M., Dehandschutter, B., Glorie, S., 2008. Apatite fission-track thermochronology applied to the Chulyshman Plateau, Siberian Altai Region. Radiation Measurements 43, 38–42.

De Grave, J., Buslov, M.M., Van den haute, P., Metcalf, J., Dehandschutter, B., Mc Williams, M.O., 2009. Multi-Method chronometry of the Teletskoye graben and its basement, Siberian Altai Mountains: new insights on its thermo-tectonic evolution. In: Lisker, F., Ventura, B., Glasmacher, U.A. (Eds.), Thermochronological methods from palaeotemperature constraints to landscape evolution models: The Geological Society of London Special Publication, 324, pp. 237–259.

De Grave, J., Glorie, S., Ryabinin, A., Zhimulev, F., Buslov, M.M., Izmer, A., Elburg, M., Vanhaecke, F., Van den haute P., (in press). Late Palaeozoic and Meso-Cenozoic tectonic evolution of the Southern Kyrgyz Tien Shan: constraints from multi-method thermochronology in the Trans-Alai, Turkestan-Alai Section and the Southeastern Ferghana Basin. Journal of Asian Earth Sciences, doi:10.1016/j.jseaes.2011.04.019.

Donelick, R.A., O'Sullivan, P.B., Ketcham, R.A., 2005. Apatite fission-track analysis. Reviews in Mineralogy and Geochemistry 58, 49–94.

Dumitru, T.A., Zhou, D., Chang, E.Z., Graham, S.A., 2001. Uplift, exhumation, and deformation in the Chinese Tian Shan. Geological Society of America Memoir 194, 71–99.

Dunkl, I., Mikes, T., Frei, D., Gerdes, A., von Eynatten, H., 2009. PepiAGE: data reduction program for time-resolved U/Pb analyses—introduction and call for tests and discussion. University of Goettingen Publication. http://www.sediment.uni-goettingen.de/staff/dunkl/zips/PepiAGE-introduction-c1.pdf. 15 pp.

Enkelmann, E., Jonckheere, R., Ratschbacher, L., 2005. The effects of radiation damage accumulation and annealing on fission-track dating of titanite. Nuclear Instruments and Methods in Physics Research B227, 567–576.

Farley, K.A., 2002. (U–Th)/He dating: techniques, calibrations, and applications: Noble Gas Geochemistry, Reviews in Mineralogy and Geochemistry, 47, pp. 819–844.

Farley, K.A., Wolf, R.A., Silver, L.T., 1996. The effects of long alpha-stopping distances on (U–Th)/He ages. Geochimica et Cosmochimica Acta 60, 4223–4229.

Fitzgerald, P.G., Stump, E., 1997. Cretaceous and Cenozoic episodic denudation of the Transantarctic Mountains, Antarctica: new constraints from apatite fission track thermochronology in the Scott Glacier region. Journal of Geophysical Research 102 (B4), 7747–7765.
Gallagher, K., Brown, R., 1997. The onshore record of passive margin evolution. Journal of the Geological Society of London 154, 451–457.
Galliker, D., Hugentobler, E., Hahn, B., 1970. Spontane kernspaltung von ^{238}U und ^{241}Am. Helveticae Physicae Acta 43, 593–606.
Gao, J., Long, L.L., Klemd, R., Qian, Q., Liu, D.Y., Xiong, X.M., Su, W., Liu, W., Wang, Y.T., Yang, F.Q., 2009. Tectonic evolution of the South Tianshan orogen and adjacent regions, NW China: geochemical and age constraints of granitoid rocks. International Journal of Earth Science 98, 1221–1238.
Gleadow, A.J.W., Fitzgerald, P.G., 1987. Uplift history and structure of the Transantarctic Mountains: new evidence from fission track dating of basement apatites in the Dry Valley area, southern Victoria Land. Earth and Planetary Science Letters 82, 1–14.
Gleadow, A.J.W., Duddy, I.R., Green, P.F., Lovering, J.F., 1986. Confined fission track lengths in apatite: a diagnostic tool for thermal history analysis. Contributions to Mineralogy and Petrology 94, 405–415.
Glorie, S., De Grave, J., Buslov, M.M., Elburg, M.A., Stockli, D.F., Van den haute, P., Gerdes, A., 2010a. Multi-method chronometric constraints on the evolution of the Northern Kyrgyz Tien Shan batholith: from emplacement to exhumation. Journal of Asian Earth Sciences 38, 131–146.
Glorie, S., De Grave, J., Van den haute, P., Elburg, M.A., 2010b. Evaluating the effect of anisotropy on fossil fission track length distributions in apatite. Abstract, Thermo2010, 12th International Conference on Thermochronology, p. 120.
Glorie, S., De Grave, J., Buslov, M.M., Zhimulev, F.I., Izmer, A., Vandoorne, W., Ryabinin, A., Van den haute, P., Elburg, M.A., 2011. Formation and Palaeozoic evolution of the Gorny-Altai - Altai-Mongolia suture zone (South Siberia): zircon U/Pb constraints on the igneous record. Gondwana Research 20, 465–484.
Gradstein, F.M., Ogg, J.G., Smith, A.G., Bleeker, W., Lourens, L.J., 2004. A new geological time scale, with special reference to Precambrian and Neogene. Episodes 27, 83–100.
Graham, S.A., Hendrix, M.S., Wang, L.B., Carroll, A.R., 1993. Collisional successor basins of western China: impact of tectonic inheritance on sand composition. Geological Society of America Bulletin 105, 323–344.
Green, P.F., 1985. Comparison of zeta calibration baselines for fission-track dating of apatite, zircon and sphene. Chemical Geology 58, 1–22.
Green, P.F., 1986. On the thermo-tectonic evolution of northern England: evidence from fission track analysis. Geological Magazine 123, 493–506.
Green, P.F., Duddy, I.R., 2006. Interpretation of apatite (U–Th)/He ages and fission track ages from cratons. Earth and Planetary Science Letters 244, 541–547.
Hendrix, M.S., 2000. Evolution of Mesozoic sandstone compositions, southern Junggar, northern Tarim, and western Turpan basins, northwest China: a detrital record of the ancestral Tian Shan. Journal of Sedimentary Research 70, 520–532.
Huntington, K.W., Ehlers, T.A., Hodges, K.V., Whipp, D.M., 2007. Topography, exhumation pathway, age uncertainties, and the interpretation of thermochronometer data. Tectonics 26, TC4012 23 pp.
Hurford, A.J., 1990. Standardization of fission track dating calibration: recommendation by the Fission Track Working Group of the I.U.G.S. Subcommission on Geochronology. Chemical Geology (Isotope Geoscience Section) 80, 171–178.
Jackson, S.E., Pearson, N.J., Griffin, W.L., Belousova, E.A., 2004. The application of laser ablation-inductively coupled plasma-mass spectrometry to in situ U–Pb zircon geochronology. Chemical Geology 211, 47–69.
Jenchuraeva, R., 2001. Paleozoic geodynamics, magmatism, and metallogeny of the Tien Shan. In: Seltmann, R., Jenchuraeva, R. (Eds.), Paleozoic geodynamics and gold deposits in the Kyrgyz Tien Shan, IGCP-373 excursion guide book, Bishkek, pp. 29–70.
Jenchuraeva, R., Bakirov, A., Ghes, M., Seltmann, R., Shatov, V., Popov, V., 2001. Mineral Deposits Map of Kyrgyzstan, 1:1,000,000. International Association on the Genesis of Ore Deposits, London-Bishkek.
Jonckheere, R.C., Wagner, G.A., 2000a. On the thermal stability of fossil and neutron-induced fission-tracks in natural titanite. Nuclear Instruments and Methods in Physics Research B168, 78–87.
Jonckheere, R.C., Wagner, G.A., 2000b. On the occurrence of anomalous fission tracks in apatite and titanite. American Mineralogist 85, 1744–1753.
Jonckheere, R., Ratschbacher, L., Wagner, G., 2003. A repositioning technique for counting induced fission tracks in muscovite external detectors in single-grain dating of minerals with low and inhomogeneous uranium concentrations. Radiation Measurements 37, 217–219.
Ketcham, R.A., 2005. Forward and inverse modeling of low-temperature thermochronometry data. Reviews in Mineralogy and Geochemistry 58, 275–314.
Ketcham, R.A., Carter, A., Donelick, R.A., Barbarand, J., Hurford, A.J., 2007. Improved modelling of fission-track annealing in apatite. American Mineralogist 92, 799–810.
Konopelko, D., Biske, G., Seltmann, R., Eklund, O., Belyatsky, B., 2007. Hercynian post-collisional A-type granites of the Kokshaal Range, Southern Tien Shan, Kyrgyzstan. Lithos 97, 140–160.
Konopelko, D., Biske, G., Seltmann, R., Kiseleva, M., Matukov, D., Sergeev, S., 2008. Deciphering Caledonian events: timing and geochemistry of the Caledonian magmatic arc in the Kyrgyz Tien Shan. Journal of Asian Earth Sciences 32, 131–141.
Konopelko, D., Seltmann, R., Biske, G., Lepekhina, E., Sergeev, S., 2009. Possible source dichotomy of contemporaneous post-collision barren I-type versus tin-bearing A-type granites, lying on opposite sides of the South Tien Shan suture. Ore Geology Reviews 35, 206–216.
Kröner, A., Alexeiev, D.V., Mikolaichuk, A., Xia, X., Zack, T., Windley, B.F., Sun, M., Rojas-Agramonte, Y., Liu, D., 2009. New single zircon ages of Precambrian and Palaeozoic rocks from the Northern, Middle and Southern Tianshan belts in Kyrgyzstan. Abstract, International Excursion and Workshop on tectonic evolution and crustal structure of the Tien Shan belt and related terrains in the Central Asian Orogenic Belt, Bishkek, 9–17 June 2009, p. 30.
Ludwig, K., 2003. User's Manual for Isoplot 3.00, A Geochronological Toolkit for Microsoft Excel. : Berkeley Geochronology Center Special Publication, v. 4.
Maksumova, R.A., Dzhenchuraeva, A.V., Berezanskii, A.V., 2001. Structure and evolution of the Tien Shan nappe-folded orogen. Russian Geology and Geophysics 42, 1367–1374.
Mao, J., Konopelko, D., Seltmann, R., Lehmann, B., Chen, W., Wang, Y., Eklund, O., Usubaliev, T., 2004. Postcollisional age of the Kumtor gold deposit and timing of Hercynian events in the Tien Shan, Kyrgyzstan. Economic Geology 99, 1771–1780.
Mikolaichuk, A.V., Kurenkov, S.A., Degtyarev, K.E., Rubtsov, V.I., 1997. Northern Tien Shan main stages of geodynamic evolution. Geotectonics 31, 445–462.
Molnar, P., Tapponnier, P., 1975. Cenozoic tectonics of Asia: effects of a continental collision. Science 189, 419–426.
Omuralieva, A., Nakajima, J., Hasegawa, A., 2009. Three-dimensional seismic velocity structure of the crust beneath the central Tien Shan, Kyrgyzstan: implications for large- and small-scale mountain building. Tectonophysics 465, 30–44.
Otto, S.C., 1997. Mesozoic–Cenozoic history of deformation and petroleum systems in sedimentary basins of Central Asia: implications of collisions on the Eurasian margin. Petroleum Geoscience 3, 327–341.
Pirajno, F., 2010. Intracontinental strike-slip faults, associated magmatism, mineral systems and mantle dynamics: examples from NW China and Altay-Sayan (Siberia). Journal of Geodynamics 50, 325–346.
Schwab, M., Ratschbacher, L., Siebel, W., McWilliams, M., Minaev, V., Lutkov, V., Chen, F., Stanek, K., Nelson, B., Frisch, F., Wooden, J.L., 2004. Assembly of the Pamirs: age and origin of magmatic belts from the southern Tien Shan to the southern Pamirs and their relation to Tibet. Tectonics 23, TC4002. doi:10.1029/2003TC001583 31 pp.
Seltmann, R., Konopelko, D., Biske, G., Divaev, F., Sergeev, S., in press. Hercynian post-collisional magmatism in the context of Paleozoic magmatic evolution of the Tien Shan orogenic belt. Journal of Asian Earth Sciences, doi:10.1016/j.jseaes.2010.08.016.
Shuster, D.L., Flowers, R.M., Farley, K.A., 2006. The influence of natural radiation damage on helium diffusion kinetics in apatite. Earth and Planetary Science Letters 249, 148–161.
Sláma, J., Košler, J., Condon, D.J., Crowley, J.L., Gerdes, A., Hanchar, J.M., Horstwood, M.S.A., Morris, G.A., Nasdala, L., Norberg, N., Schaltegger, U., Schoene, B., Tubrett, M.N., Whitehouse, M.J., 2008. Plešovice zircon—a new natural reference material for U–Pb and Hf isotopic microanalysis. Chemical Geology 249, 1–35.
Sobel, E.R., Seward, D., 2010. Influence of etching conditions on apatite fission-track etch pit diameter. Chemical Geology 271, 59–69.
Sobel, E.R., Hilley, G.E., Strecker, M.R., 2003. Formation of internally drained contractional basins by aridity-limited bedrock incision. Journal of Geophysical Research 108 (B7), 2344 23 pp.
Sobel, E., Chen, J., Heermance, R.V., 2006a. Late Oligocene–Early Miocene initiation of shortening in the SW Chinese Tian Shan: implications for Neogene shortening rate variations. Earth and Planetary Science Letters 247, 70–81.
Sobel, E.R., Oskin, M., Burbank, D., Mikolaichuk, A., 2006b. Exhumation of basement-cored uplifts: example of the Kyrgyz Range quantified with apatite fission track thermochronology. Tectonics 25, 1–17.
Solomovich, L.I., 2007. Postcollisional magmatism in the South Tien Shan Variscan Orogenic Belt, Kyrgyzstan: evidence for high-temperature and high-pressure collision. Journal of Asian Earth Sciences 30, 142–153.
Spiegel, C., Kohn, B., Belton, D., Berner, Z., Gleadow, A., 2009. Apatite (U–Th–Sm)/He thermochronology of rapidly cooled samples: the effect of He implantation. Earth and Planetary Science Letters 285, 105–114.
Stacey, J.S., Kramers, J.D., 1975. Approximation of terrestrial lead isotope evolution by a two-stage model. Earth and Planetary Science Letters 26, 207–221.
Stockli, D.F., Farley, K.A., Dumitru, T.A., 2000. Calibration of the apatite (U–Th)/He thermochronometer on an exhumed fault block, White Mountains, California. Geology 28, 983–986.
Tian, W., Campbell, I.H., Allen, C.M., Guan, P., Pan, W., Chen, M., Yu, H., Zhu, W., 2010. The Tarim picrite–basalt–rhyolite suite, a Permian flood basalt from northwest China with contrasting rhyolites produced by fractional crystallization and anatexis. Contributions to Mineralogy and Petrology 160, 407–425.
Tursungaziev, B.T., Petrov, O.B., 2008. Geological map of the Kyrgyz Republic, 1:500,000. Agency of Geology and Mineralogical Resources of the Kyrgyz Republic, Bishkek.
Van der Beek, P.A., Valla, P.G., Herman, F., Braun, J., Persano, C., Dobson, K.J., Labrin, E., 2010. Inversion of thermochronological age-elevation profiles to extract independent estimates of denudation and relief history—II: application to the French Western Alps. Earth and Planetary Science Letters 296, 9–22.
Vincent, S.J., Allen, M.B., 2001. Sedimentary record of Mesozoic intracontinental deformation in the eastern Junggar Basin, northwest China: response to orogeny at the Asian margin. Geological Society of America Memoir 194, 341–360.
Wagner, G.A., Van den haute, P., 1992. Fission Track-Dating. Kluwer Academic Publishers, Dordrecht, the Netherlands. 285 pp.
Wiedenbeck, M., Alle, P., Corfu, F., Griffin, W., Meier, M., Oberli, F., von Quadt, A., Roddick, J.C., Spiegel, W., 1995. Three natural zircon standards for U–Th–Pb, Lu–Hf, trace element and REE analysis. Geostandards Newsletter 19, 1–23.
Williams, I.S., Tetley, N.W., Compston, W., McDougall, I., 1982. A comparison of K–Ar and Rb–Sr ages of rapidly cooled igneous rocks: two points in the Paleozoic time scale re-evaluated. Journal of the Geological Society of London 139, 557–568.
Windley, B.F., Alexeiev, D., Xiao, W., Kröner, A., Badarch, G., 2007. Tectonic models for accretion of the Central Asian Orogenic Belt. Journal of the Geological Society of London 164, 31–47.
Xiao, W.J., Windley, B.F., Huang, B.C., Han, C.M., Yuan, C., Chen, H.L., Sun, M., Sun, S., Li, J.L., 2009. End-Permian to mid-Triassic termination of the accretionary processes of the

southern Altaids: implications for the geodynamic evolution, Phanerozoic continental growth, and metallogeny of Central Asia. International Journal of Earth Science 98, 1189–1217.

Xiao, W.J., Huang, B.C., Han, C.M., Sun, S., Li, J.L., 2010. A review of the western part of the Altaids: a key to understanding the architecture of accretionary orogens. Gondwana Research 18, 253–273.

Zhang, C.-L., Li, Z.-X., Li, X.-H., Ye, H.-M., Li, C.-N., 2008. A Permian layered intrusive complex in the western Tarim Block, NW China: product of a ca. 275 Ma mantle plume? The Journal of Geology 116, 269–287.

Zhang, Y., Liu, J., Guo, Z., 2010. Permian basaltic rocks in the Tarim basin, NW China: implications for plume–lithosphere interaction. Gondwana Research 18, 596–610.